The Plant Cell, Vol. 23: 2788–2803, July 2011, www.plantcell.org © 2011 American Society of Plant Biologists. All rights reserved.

Perturbation of *Arabidopsis* Amino Acid Metabolism Causes Incompatibility with the Adapted Biotrophic Pathogen *Hyaloperonospora arabidopsidis* [C][W][OA]

Johannes Stuttmann,[a] Hans-Michael Hubberten,[b] Steffen Rietz,[a,1] Jagreet Kaur,[a,2] Paul Muskett,[a] Raphael Guerois,[c] Paweł Bednarek,[a] Rainer Hoefgen,[b] and Jane E. Parker[a,3]

[a] Department of Plant-Microbe Interactions, Max Planck Institute for Plant Breeding Research, D-50829 Cologne, Germany
[b] Max Planck Institute of Molecular Plant Physiology, D-14476 Potsdam-Golm, Germany
[c] Commissariat á l'Energie Atomique, Institut de Biologie et Technologies de Saclay, Laboratoire de Biologie Structurale et Radiobiologie and Centre National de la Recherche Scientifique, Unités de Recherche Associées 2096, F-91191 Gif-sur-Yvette, France

Reliance of biotrophic pathogens on living plant tissues to propagate implies strong interdependence between host metabolism and nutrient uptake by the pathogen. However, factors determining host suitability and establishment of infection are largely unknown. We describe a loss-of-inhibition allele of *ASPARTATE KINASE2* and a loss-of-function allele of *DIHYDRODIPICOLINATE SYNTHASE2* identified in a screen for *Arabidopsis thaliana* mutants with increased resistance to the obligate biotrophic oomycete *Hyaloperonospora arabidopsidis* (*Hpa*). Through different molecular mechanisms, these mutations perturb amino acid homeostasis leading to overaccumulation of the Asp-derived amino acids Met, Thr, and Ile. Although detrimental for the plant, the mutations do not cause defense activation, and both mutants retain full susceptibility to the adapted obligate biotrophic fungus *Golovinomyces orontii* (*Go*). Chemical treatments mimicking the mutants' metabolic state identified Thr as the amino acid suppressing *Hpa* but not *Go* colonization. We conclude that perturbations in amino acid homeostasis render the mutant plants unsuitable as an infection substrate for *Hpa*. This may be explained by deployment of the same amino acid biosynthetic pathways by oomycetes and plants. Our data show that the plant host metabolic state can, in specific ways, influence the ability of adapted biotrophic strains to cause disease.

INTRODUCTION

Plant-infecting microbes have evolved diverse lifestyles to survive changing environments and host selection pressures. The success of many pathogens depends on a high degree of specialization to a particular plant host which, at the same time, can restrict their host range (Kämper et al., 2006; Tyler et al., 2006). Non-host resistance, defined as immunity of an entire plant species against all genetic variants of a pathogen species, is one major host range-limiting factor. In *Arabidopsis thaliana*, non-host resistance has been shown to depend on the rapid mobilization of vesicles and defense-associated proteins to attempted invasion sites (Kwon et al., 2008; Wang et al., 2009). Also, chemical responses involving the Trp-derived phytoalexin camalexin and indolic glucosinolates protect cells against attempted infection by biotrophic and necrotrophic pathogens (Bednarek et al., 2009; Sanchez-Vallet et al., 2010; Schlaeppi et al., 2010). As a consequence, mutant plants defective in two redundant CYP79B monooxygenases catalyzing the conversion of Trp to indole-3-acetaldoxime, and thus lacking Trp-derived secondary metabolites, support increased growth of normally nonadapted pathogen isolates (Sanchez-Vallet et al., 2010; Schlaeppi et al., 2010).

Host-adapted pathogens have evolved the ability to overcome non-host defenses and successfully colonize plant tissues. Effector molecules produced by infectious microbes are known to suppress plant defenses or manipulate host development in favor of pathogen growth (reviewed in Bent and Mackey, 2007). In a coevolutionary conflict with the host, some effectors become recognized by intracellular nucleotide binding site–leucine-rich repeat–containing immune sensors (NLRs). As a pathogen effector-driven process, receptor-mediated (race-specific) resistance depends on the genetic repertoire of the host and adapted pathogen (Bent and Mackey, 2007). NLR activation upon direct or indirect recognition of an effector molecule induces a signaling cascade leading to pathogen containment often involving host programmed cell death (the hypersensitive response [HR]) and accumulation of the systemic resistance signaling hormone salicylic acid (SA) (Bent and Mackey, 2007; Vlot et al., 2009). Many NLRs additionally require HSP90 and its

[1] Current address: Christian-Albrechts-Universität Kiel, Department of Molecular Phytopathology, Herrmann-Rodewald-Str. 9, 24118 Kiel, Germany.
[2] Current address: Department of Genetics, University of Delhi South Campus, Benito Juarez Road, Dhaula Kuan, New Delhi 110 021, India.
[3] Address correspondence to parker@mpipz.mpg.de.
The author responsible for distribution of materials integral to the findings presented in this article in accordance with the policy described in the Instructions for Authors (www.plantcell.org) is: Jane E. Parker (parker@mpipz.mpg.de).
[C]Some figures in this article are displayed in color online but in black and white in the print edition.
[W]Online version contains Web-only data.
[OA]Open Access articles can be viewed online without a subscription.
www.plantcell.org/cgi/doi/10.1105/tpc.111.087684

cochaperones SGT1 and RAR1 for stability and/or activation (Shirasu, 2009; Zhang et al., 2010).

The obligate biotrophic oomycete pathogen *Hyaloperonospora arabidopsidis* (*Hpa*) has become specialized to infect *Arabidopsis*, causing downy mildew disease. Coadaptation within this natural pathosystem is reflected by the extensive genetic variation in responses of different *Arabidopsis* accessions to *Hpa* isolates (Holub et al., 1994). Oomycetes are distinct from true fungi in that they possess a cellulose-based cell wall with little or no chitin and are phylogenetically close to brown algae and diatoms within the Stramenopile (heterokont) lineage (reviewed in Coates and Beynon, 2010). On susceptible *Arabidopsis* accessions, *Hpa* asexual conidospores can germinate on leaves to produce a ramifying intercellular network of hyphae with haustorial invaginations of individual host cells believed to serve as specialized feeding structures (Coates and Beynon, 2010). As an obligate biotrophic parasite, *Hpa* is adept at maintaining host cell viability and integrity, most likely through the collective activities of protein effectors, some of which are translocated across the haustorial and host cell membranes into the plant cytoplasm (Whisson et al., 2007; Kale et al., 2010). The *Hpa* life cycle is completed by formation of conidiospores on the leaf surface and generation of longer lived sexual oospores inside leaves (Coates and Beynon, 2010). NLR recognition of specific *Hpa* effectors on resistant *Arabidopsis* accessions leads to a typical HR and accumulation of SA (Vlot et al., 2009; Coates and Beynon, 2010).

The absolute dependence of obligate biotrophs such as *Hpa* on their hosts and the intimate physical and molecular interactions between host and pathogen structures implies that additional host factors besides the dedicated defense machinery may be decisive for infection. Plant factors required for host colonization by symbiotic nitrogen-fixing bacteria have been identified (e.g., Hakoyama et al., 2009). Plant susceptibility determinants for biotrophic pathogen colonization have also been described but are not well understood. For example, successful entry of powdery mildew fungal germinating spores into host epidermal cells depends on functional MILDEW RESISTANCE LOCUS O (MLO) protein in barley (*Hordeum vulgare*) and *Arabidopsis*, although the precise function of MLO is unclear (Büschges et al., 1997; Consonni et al., 2006). Genetic screens of *Arabidopsis* identified a range of recessive *powdery mildew resistant* and *downy mildew resistant* (*dmr*) mutants that affect host cell wall composition and/or stress metabolite status (reviewed in O'Connell and Panstruga, 2006). *dmr1*, mediating strong and specific resistance to *Hpa*, encodes homoserine kinase, a chloroplast enzyme involved in the biosynthesis of the Asp-derived amino acids Met, Thr, and Ile (van Damme et al., 2009). *dmr1* mutants accumulated high levels of homoserine (HS), and treatment of plants with HS induced resistance to *Hpa* but did not interfere with *Hpa* spore germination or radial growth of the hemibiotrophic oomycete *Phytophthora capsici* in vitro (van Damme et al., 2009). The mechanism underlying increased downy mildew resistance through accumulation of HS in the chloroplast was not defined (van Damme et al., 2009).

Here, we describe the characterization of two nonallelic *Arabidopsis* mutants that display enhanced resistance to host-adapted *Hpa*. These mutants were identified in a screen for genetic suppressors of susceptibility to *Hpa* (isolate Noco2) caused by a *rar1* mutation disabling *RPP5* (NLR) recognition (Muskett et al., 2002). The *rar1 suppressor* (*rsp*) mutations cause perturbations of plant amino acid homeostasis by different molecular mechanisms, leading to strong and specific resistance to *Hpa*. In contrast with the induced defense programs triggered by *Hpa* effector recognition, we find that suppression of *Hpa* growth on *rsp* mutants is a result of Thr accumulation rendering host tissues unsuitable as a growth substrate. The metabolic state provoked by the *rsp* mutations is also detrimental for the plant, and specific loss of susceptibility to adapted *Hpa* isolates in the *rsp* mutants might be explained by deployment of the same metabolic pathway in the phylogenetically related oomycete. Our data suggest that host metabolic status can influence the range of biotrophic pathogens causing disease.

RESULTS

Mutants with Altered Responses to *Hpa*

Complete resistance in *Arabidopsis* accession Landsberg *erecta* (L*er*) to *Hpa* isolate Noco2 mediated by *RPP5* (Parker et al., 1993) depends on *RAR1*, encoding an HSP90 cochaperone (Muskett et al., 2002; Zhang et al., 2010). We used the intermediate resistance phenotype of a partially defective *rar1* mutant, *rar1-15*, as a sensitized background for a forward genetic screen to identify mutants with an altered response to Noco2 infection. Seeds of *rar1-15* were ethyl methanesulfonate mutagenized, and ~2600 M2 families derived from single M1 plants screened for enhanced (*rar1 enhancer* [*ren*]) or reduced (*rsp*) susceptibility to *Hpa* Noco2. A number of *ren* and *rsp* mutants were selected for further characterization. Here, we describe analysis of two nonallelic *rsp* mutants, *rsp1* and *rsp2*. Increased resistance of *rsp1* and *rsp2* to *Hpa* Noco2 was maintained after crossing into the *rar1-13* null mutant background, indicating that the resistance does not depend on a partially functional rar1-15 protein. We used the *rar1-13 rsp1* and *rar1-13 rsp2* mutants for further characterization of *rsp1* and *rsp2* phenotypes. When infected with *Hpa* isolate Noco2, pathogen growth and sporulation were seen on L*er rar1-13*, contrasting with the complete resistance associated with an HR in wild-type L*er*, visualized microscopically after trypan blue (TB) staining of leaves (Figure 1A). The *rar1-13 rsp1* and *rar1-13 rsp2* double mutants exhibited strong resistance to *Hpa*. Whereas limited pathogen growth was occasionally observed in leaves of *rar1-13 rsp1*, there were no symptoms of disease or host cell death in *rar1-13 rsp2* plants (Figure 1A). The absence of HR lesions in *rar1-13 rsp2* was especially evident when infected plants were observed under UV light (see Supplemental Figure 1A online). To test whether the increased resistance of *rar1-13 rsp1* and *rar1-13 rsp2* was dependent on *RPP5*, we infected the mutants with the virulent *Hpa* isolate Cala2, which is not recognized by *RPP5*. As expected, enhanced Cala2 sporulation was observed on *rar1-13* and *eds1-2* compared with wild-type L*er* (Figure 1B). *eds1-2* is defective in downstream signaling after activation of NLRs containing an N-terminalToll/interleukin-1 receptor domain (Aarts et al., 1998; Wirthmueller et al., 2007) and was included in pathogenicity assays as a mutant with

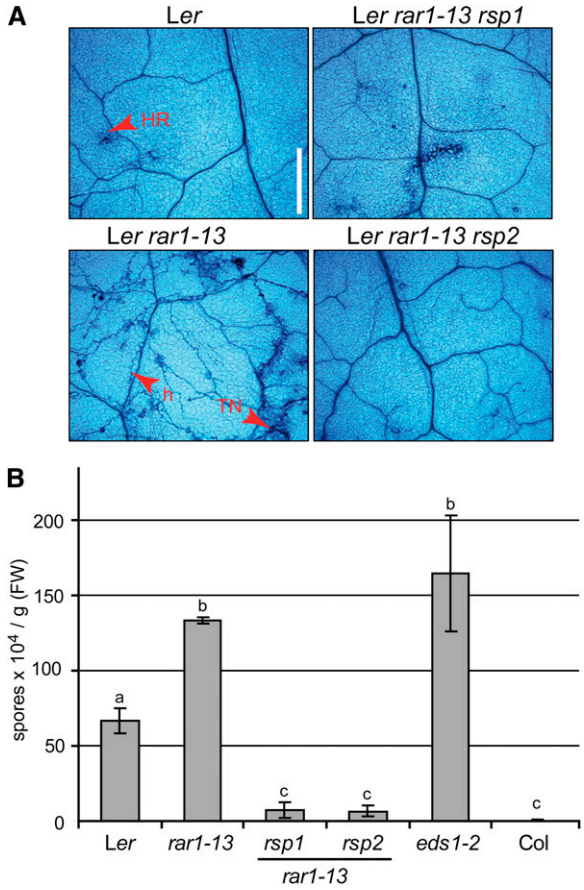

Figure 1. *rsp1* and *rsp2* Confer Strong Resistance against Different *Hpa* Isolates.

(A) Disease symptom formation on *rsp* mutant leaves. Three-week-old plants were infected with *Hpa* isolate Noco2, and first true leaves were stained with TB at 7 d after inoculation and examined under a light microscope. h, hyphae; TN, trailing necrosis. Bar = 0.5 mm.

(B) Conidiospore formation 6 d after infection of 3-week-old plants with *Hpa* isolate Cala2. Accession Col was included as a control expressing *RPP2* resistance to Cala2. Standard deviations of three biological replicates are shown. Significantly different classes are indicated by lowercase letters (one-way ANOVA, Tukey's post-hoc test, $P < 0.05$ each). FW, fresh weight.

high susceptibility. By contrast, pathogen sporulation was strongly reduced on *rar1-13 rsp1* and *rar1-13 rsp2* mutant plants that grouped statistically with the fully resistant Columbia-0 (Col-0) accession (Figure 1B). We concluded that the mutations in *rsp1* and *rsp2* cause reduced susceptibility to *Hpa* infection independently of *RPP5*.

rsp1 and *rsp2* Are Not Constitutive Resistance Mutants

The *rar1-13 rsp1* and *rar1-13 rsp2* mutants are smaller than wild-type L*er* or *rar1-13* when grown under normal conditions in soil (see Supplemental Figure 1B online). This feature, together with their reduced susceptibility to a virulent *Hpa* isolate, suggested they may be expressing constitutive resistance, which is normally accompanied by growth retardation, increased steady state accumulation of SA, and expression of *Pathogenesis-Related* (*PR*) genes leading to broad spectrum resistance (e.g., Lu et al., 2003; Zhang et al., 2003). We therefore tested for hallmarks of constitutive resistance. Free and total SA levels were reduced in *rar1-13* compared with the wild type. In *rar1-13 rsp1* and *rar1-13 rsp2*, SA accumulation was intermediate between wild-type L*er* and *rar1-13* (Figure 2A) and therefore not characteristic of constitutive resistance mutants. We then tested whether the enhanced *Hpa* resistance of the *rsp* mutants might correlate with increased basal expression or accelerated *PR* gene induction upon infection that would reflect priming of defenses (Conrath et al., 2002). Plants were infected with *Hpa* isolate Noco2. Samples were taken up to 72 h after inoculation and expression of the SA-responsive *PR* gene *PR1* measured by quantitative RT-PCR. Individual analysis of variance (ANOVA) tests detected significant *PR1* induction over time in all genotypes (Figure 2B). No significant differences in *PR1* expression were detected between *rar1-13*, *rar1-13 rsp1*, and *rar1-13 rsp2* (Figure 2B). These data show that the increased resistance of the *rar1-13 rsp* mutants cannot be explained by enhanced basal or *Hpa*-induced SA defenses. We infected plants with a virulent strain (DC3000) of the bacterial pathogen *Pseudomonas syringae* pv *tomato* (*Pst*) to test whether increased resistance of *rar1-13 rsp* mutants extended to an unrelated hemibiotrophic pathogen. *Pst* DC3000 grew more in *rar1-13* and *eds1-2* compared with L*er* wild type, as expected (Figure 2C; Muskett et al., 2002). The *rar1-13 rsp1* and *rar1-13 rsp2* double mutants supported similar (*rsp1*) or higher (*rsp2*) bacterial growth compared with *rar1-13* (Figure 2C). These data argue against the *rsp* mutations causing constitutive disease resistance.

To test whether increased resistance to *Hpa* observed in the *rar1-13 rsp* mutants extends to a different host-adapted obligate biotrophic pathogen, we inoculated plants with the adapted powdery mildew fungus *Golovinomyces orontii* (*Go*). Fungal entry into *Arabidopsis* epidermal cells is used as an indicator of early infection competence. The host cell entry rate of *Go* in *rar1-13 rsp1* and *rar1-13 rsp2* cells was therefore compared with that in wild-type L*er* and the *rar1-13* single mutant. Accession Col (susceptible) and the Col *mlo2-6* (*MILDEW RESISTANCE LOCUS O2*) mutant, which is more resistant to *Go* (Consonni et al., 2006), were included as additional controls in the experiment. Fungal host entry rates were similar in Col and L*er* and not altered by the *rar1-13*, *rsp1*, or *rsp2* mutations, but significantly reduced in *mlo2-6* (Figure 2D). Development of macroscopic disease symptoms was evaluated between 4 and 7 d after infection. There was enhanced sporulation on *rar1-13 rsp2* plants compared with L*er* and *rar1-13* (see Supplemental Figure 2 online). Symptom formation on *rar1-13 rsp1* was accompanied by leaf yellowing but *Go* sporulation itself was not altered. As expected, sporulation on *mlo2-6* was reduced compared with Col (see Supplemental Figure 2 online). Since resistance of the *rsp* mutants does not extend to another host-adapted biotrophic pathogen, we concluded that the *rsp1* and *rsp2* defects perturb the *Arabidopsis–Hpa* interaction in quite a specific manner. This prompted us to clone and characterize the *RSP1* and *RSP2* genes.

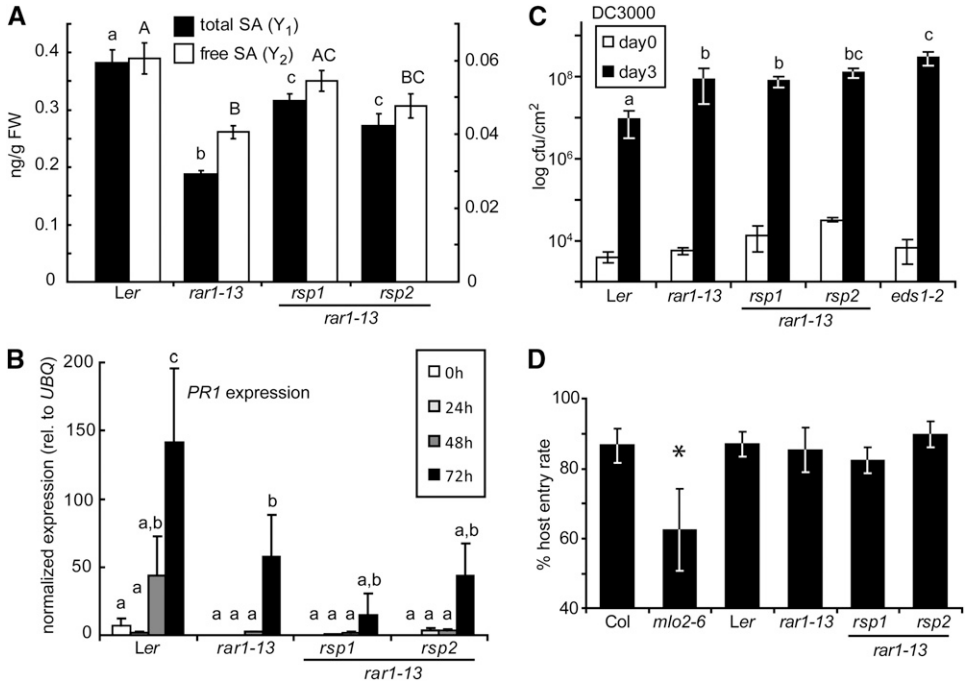

Figure 2. *rsp1* and *rsp2* Are Not Constitutive Resistance Mutants.

(A) Steady state SA accumulation in 4-week-old plants. Total (black bars, Y1) and free (white bars, Y2) SA was extracted from leaf tissue and measured by GC-MS. Standard deviations of three samples are shown. Letters indicate classes separated by significant differences (one-way ANOVA, Tukey's post-hoc test, $P < 0.05$ each): lower-case, total SA; upper-case, free SA. FW, fresh weight.

(B) *PR1* induction by *Hpa*. Three-week-old plants were infected with *Hpa* isolate Noco2 and samples taken at the indicated time points. Expression of *PR1* and *UBQ10* was determined by quantitative RT-PCR. Relative expression of *PR1* normalized to *UBQ* in each sample is displayed, and error bars indicate standard deviations of three independent samples. Significantly different classes are indicated by lower-case letters (repeated measures ANOVA, Tukey's post-hoc test, $P < 0.05$ each).

(C) Growth of *Pst* DC3000 on *rsp* mutant plants. The indicated lines were spray infected with bacteria at 4×10^5 colony-forming units (cfu) per mL. Bacterial growth (cfu/cm^2) was determined 1 h (white bars) and 3 d (black bars) after infection. Error bars represent standard deviations of four samples. Significantly different classes are indicated by lower-case letters (one-way ANOVA, Tukey's post-hoc test, $P < 0.05$ each).

(D) Host entry rate of *G. orontii*. Entry rates on the indicated plant lines were determined from Coomassie blue–stained leaves 2 d after infection of 6-week-old plants. Standard deviations of at least five counts from different leaves are shown. Asterisk indicates significant differences (one-way ANOVA, Tukey's post-hoc test, $P < 0.05$ each).

rsp2 Is a Loss-of-Function Allele of *DIHYDRODIPICOLINATE SYNTHASE2*

When backcrossed *rar1-13 rsp2/RSP2* plants were selfed, resistance to *Hpa* Noco2 segregated in a 1:3 ratio (29^R:108^S; $\chi^2 = 1.07$) in the progeny indicative of a monogenic recessive trait. *rar1-13 rsp2* was crossed to the Col *rar1-28* null mutant to generate segregating F2 families for map-based cloning. Although *RPP5* also segregates in the progeny (Parker et al., 1997), we observed a clear 1:3 ratio of resistant to susceptible plants in the mapping population consistent with the enhanced resistance of *rsp2* being largely independent of *RPP5* (Figure 1B). Linkage between *rsp2* resistance and the *erecta* morphology was found and *rsp2* was mapped in ~600 phenotyped F2 plants to an 86-kb interval on the lower arm of chromosome 2. This interval contains 26 annotated genes. DNA sequencing revealed a G-to-A exchange in the coding region of *DIHYDRODIPICOLINATE SYNTHASE2* (*DHDPS2*, *At2g45440*), resulting in a predicted exchange of Gly-243 to Glu in DHDPS2 (Figures 3A and 3B).

DHDPS enzymes catalyze the formation of dihydrodipicolinate from L-aspartate-4-semialdehyde (ASA) as the committing step for biosynthesis of Lys in the biosynthesis of the Asp-derived amino acids Lys, Met, Thr, and Ile, also called the Lys superpathway (Jander and Joshi, 2010; see also scheme in Figure 5A). All reactions of this pathway from Asp phosphorylation to the amino acid end products Lys, Thr, Met, and Ile take place in the chloroplast (Ravanel et al., 2004). The mutated Gly residue in *rsp2* is highly conserved among DHDPS proteins (Figure 3B) and has a high bias in the DHDPS motif (http://pfam.sanger.ac.uk/family?acc=DHDPS#tabview=tab3). The recessive nature of *rsp2* suggests it is a reduced or loss-of-function (LOF) allele of *DHDPS2*. To test this, we searched for additional *Arabidopsis dhdps2* mutations. From several candidate T-DNA insertions in *DHDPS2* (http://signal.salk.edu/cgi-bin/tdnaexpress), one insertion in the 5′ untranslated region of *DHDPS2* was confirmed (Figure 3A). Homozygous plants of this line exhibited strong resistance compared with a control line containing the wild-type *DHDPS2* locus isolated from the same population (Figure 3C).

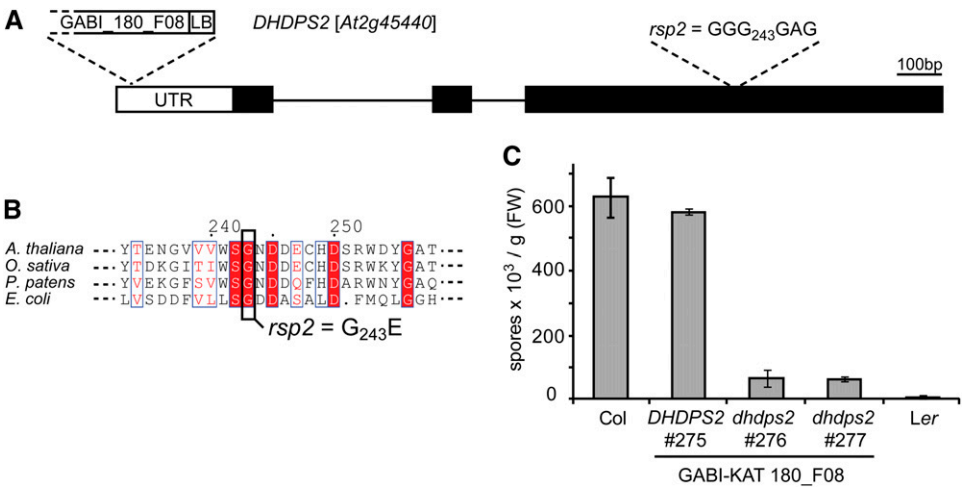

Figure 3. Molecular Cloning of the *rsp2* Mutation.

(A) Organization of the *DHDPS2* locus. Positions of the *rsp2* mutation and T-DNA insertion in GABI_180_F08 are indicated. LB, left border.
(B) Alignment of DHDPS2 proteins and position of the amino acid exchange in *rsp2*. (*At*, Q0WSN6; *Os*, Q7XPB5; *Pp*, A9SGY8; *Ec*, C9QPU6).
(C) Conidiospore formation 7 d after infection of 3-week-old plants with *Hpa* isolate Noco2. Biological replicates were pooled and treated as one sample. Error bars are derived from five technical replicates. FW, fresh weight.
[See online article for color version of this figure.]

We therefore concluded that *rsp2* is a LOF allele of *DHDPS2* and the mutant was renamed *dhdps2-2*.

The *Arabidopsis* genome contains two genes encoding DHDPS enzymes (http://www.Arabidopsis.org). To test whether DHDPS1 also contributes to *Hpa* resistance, a T-DNA insertion mutant in *DHDPS1* (*At3g60880*) was isolated (see Supplemental Figure 3 online). Insertion of the T-DNA in an exon strongly reduced *DHDPS1* transcript abundance measured by RT-PCR, suggesting that this line is a null *dhdps1* mutant. In contrast with *dhdps2-2* (*rsp2*), homozygous *dhdps1-1* mutant plants did not exhibit reduced susceptibility to *Hpa* Noco2 (see Supplemental Figure 3 online).

rsp1 Carries a Mutation in *ASPARTATE KINASE2*

The *rsp1* phenotype was initially scored as a recessive monogenic trait and crossed to Col *rar1-28* for mapping. However, scoring of mapping populations infected with *Hpa* Noco2 revealed that resistance was not strictly recessive and, depending on the infection conditions could appear dominant, suggesting dosage effects. *rsp1* was placed on the upper arm of chromosome 5 and a high-confidence interval of 360 kb containing 143 annotated loci was defined using a mapping population of ~500 phenotyped F2 plants. From this interval, a locus encoding ASPARTATE KINASE2 (*AK2*, *At5g14060*) was sequenced because *rsp1* and *rsp2*/*dhdps2-2* share common developmental defects (see Supplemental Figures 1 and 4 online), and we therefore suspected the mutations may affect the same pathway (see Figure 5A). A G-to-A exchange resulting in a predicted change of Val-430 to Met in AK2 was detected (Figures 4A and 4B). Asp kinases catalyze the conversion of Asp to L-aspartyl-4-phosphate as the first step of the Lys superpathway. The *Arabidopsis* genome contains three genes encoding monofunctional Asp kinases and two genes encoding bifunctional aspartate kinase/homoserine dehydrogenase (HSDH) enzymes (Figure 5A). Little is known about the in vivo roles of the different isoenzymes, but kinetic parameters in vitro are well described (Curien et al., 2005, 2007). The monofunctional AK2 and AK3 enzymes are allosterically inhibited by Lys, while AK1 is synergistically inhibited by Lys and *S*-adenosylmethionine. The recently reported crystal structure of the *Arabidopsis* AK1 dimer revealed binding of both effectors to its ACT1 domain (Mas-Droux et al., 2006). We built a structural model for the AK2 dimer using the AK1 crystal structure as a template (Figure 4C). The Val-430 residue mutated in *rsp1*, which is not completely conserved among AK enzymes from phylogenetically distant organisms, is located at a homodimer interface built by the two ACT1 domains, and contacts the Val-430 in the other monomer (Figure 4C). Hence, the *rsp1* mutation might interfere with AK2 protein function by impairing homodimerization, although the mutation $V_{430}M$ could be modeled without provoking major steric clashes. We isolated a putative *AK2* LOF allele from the T-DNA collections in accession Col in which the T-DNA insertion is located in an exon upstream of the mutation detected in *rsp1* (Figure 4B; see Supplemental Figure 5 online). Homozygous Col *ak2* plants were as susceptible as wild-type Col when tested with *Hpa* Noco2 (see Supplemental Figure 5B online). Therefore, we reasoned that *rsp1* is not a LOF allele of *AK2*. This is further supported by the presence of a Met residue at the same position in an AK from *Streptococcus equi* (YP_002743803). Val-430 is also very close to the binding site of the allosteric Lys molecule in AK1, which is conserved with that of the Lys-inhibited *Escherichia coli* enzyme (Mas-Droux et al., 2006). We therefore reasoned that the $V_{430}M$ mutation might instead affect feedback inhibition of the enzyme in vivo in accordance with the nonrecessivity of *rsp1* resistance.

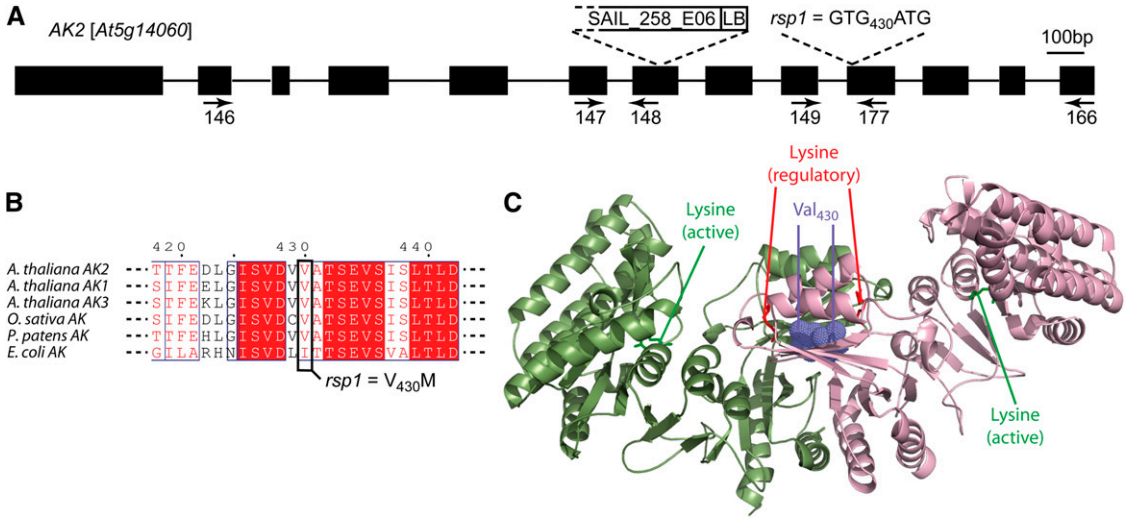

Figure 4. *rsp1* Carries a Mutation in *AK2*.

(A) Organization of the *AK2* locus. Positions of the mutation detected in *rsp1*, the T-DNA insertion in SAIL_258_06, and primers used for the RT-PCR analysis shown in Supplemental Figure 5 online are indicated. LB, left border.

(B) Alignment of AK2 proteins and position of the amino acid exchange in *rsp1* (At AK1, NP_196832; At AK2, O23653; At AK3, NP_186851; *Os*, Q6YS33; *Pp*, A9T456; *Ec*, D3QK31).

(C) Structural model of AK2 generated with AK1 as template. Homodimer subunits are shown in light green and pink. A Lys residue that was cocrystallized in the active site of the original AK1 structure and the inhibitory Lys residue are shown in green and red in each subunit (sticks depiction). The Val-430 residue is highlighted in violet as dotted spheres.

Both *rsp1* and *rsp2/dhdps2-2* Strongly Perturb Amino Acid Homeostasis

Large differences in accumulation of products of the Lys superpathway have been reported for the previously characterized *dhdps2-1* mutant (Craciun et al., 2000; Sarrobert et al., 2000). We investigated whether this is also the case for our newly identified *rsp2/dhdps2-2* mutant and possibly *rsp1*. Polar metabolite extracts from aerial tissue of soil-grown plants were therefore prepared and analyzed by gas chromatography–mass spectrometry (GC-MS). Relative peak areas for signals corresponding to Lys, Ile, Met, and Thr were determined and normalized to L*er* wild type, which was set at 100% (Figure 5B). No significant changes were detected between the wild type and *rar1-13*. In *rsp2/dhdps2-2*, higher accumulation of all pathway end products was observed, except Lys, which remained unchanged. Remarkably, a 60-fold increase in Thr levels was detected in *rsp2/dhdps2-2* compared with the wild type. The amino acid profile of *rsp1* was similar to *rsp2/dhdps2-2* except that Lys levels increased three- to fourfold (Figure 5B). Altered amino acid levels, including Lys in *rsp1* mutant plants, are consistent with our hypothesis that the rsp1 mutant protein has altered inhibition properties leading to deregulated flux of Asp, since the two DHDPS enzymes are normally tightly regulated by feedback inhibition through Lys (Craciun et al., 2000; Vauterin et al., 2000).

rsp1 Is a Loss-of-Inhibition Allele of *AK2*

We tested whether the AK2 $V_{430}M$ mutation in *rsp1* could indeed give rise to an enzyme refractive to Lys inhibition by expressing wild-type AK2 and mutant AK2^{rsp1} proteins lacking the chloroplast targeting peptide in *E. coli* as C-terminal fusions to glutathione *S*-transferase (GST). Affinity-purified GST-AK2 exhibited strong AK activity when tested in the presence of saturating concentrations of Asp and ATP (80 and 20 mM, respectively), whereas reactions containing a control protein purified under the same conditions did not show activity. The observed activity was fully dependent on the presence of Asp in the reaction mixture (data not shown). Hence, the GST-tagged protein is active and could be used for inhibition assays. GST-AK2 and GST-AK2^{rsp1} activities were compared under physiological conditions (2 mM ATP and 1 mM Asp) for inhibition by Lys (Figure 6A, top graph). A decrease in activity of the wild-type enzyme was observed with low concentrations of 10 to 25 μM Lys, as previously described (Curien et al., 2007). By contrast, even high Lys concentrations (up to 250 μM) did not lead to appreciable inhibition of AK2^{rsp1} in our assays. We confirmed this result under conditions of higher substrate availability (5 mM Asp and 10 mM ATP). Although the Lys concentration range for efficient inhibition of GST-AK2 shifted, differential inhibition properties of GST-AK2^{rsp1} remained (Figure 6A, bottom graph). Thus, a considerably higher activity of the AK2^{rsp1}enzyme would be expected at physiological levels of Lys sufficient to inhibit the wild-type enzyme. We also tested whether the *AK2^{rsp1}* mutation causes accumulation of amino acids generated by the Lys superpathway in *Arabidopsis* aerial tissues by transforming Col with constructs of AK2 or AK2^{rsp1}driven by the constitutive cauliflower mosaic virus 35S promoter. In T1 plants (selected for the cotransformed BASTA resistance marker and confirmed by PCR), 4/30 *35S:AK2^{rsp1}* transformants exhibited abnormal growth reminiscent of *rsp1*,

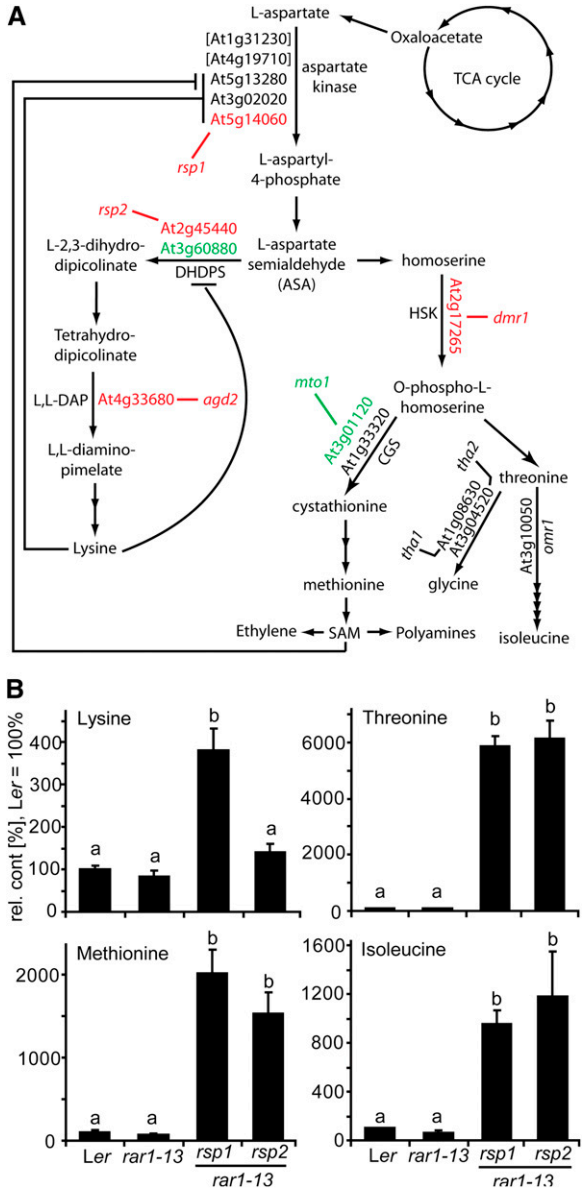

Figure 5. The Lys Superpathway and Accumulation of Its End Products in *rsp* Mutants.

(A) Scheme showing the biosynthesis of Asp-derived amino acids in *Arabidopsis*. Bifunctional AK-HSDH enzymes are shown in brackets. Allosteric inhibition mechanisms mentioned in the text are indicated with negative impacting lines. Mutants identified in this or previous studies are shown in black (not tested), red (resistant to *Hpa*), or green (no resistance phenotype). TCA, tricarboxylic acid.

(B) Accumulation of the Asp-derived amino acids Lys, Met, Thr, and Ile in *rsp* mutant and control plants. Polar metabolites were extracted from aerial tissue of 4-week-old soil-grown plants and analyzed by GC-MS. Values were normalized to L*er* = 100%, and standard deviations from three independent samples are shown. Significantly different classes are indicated by lower-case letters (one-way ANOVA, Tukey's post-hoc test, $P < 0.05$ each). Trends were confirmed in an independent experiment.

whereas all *35S:AK2* transformants (>30) grew normally (see Supplemental Figure 6 online). Thr accumulation in aerial tissues of individual *35S:AK2* and *35S:AK2^{rsp1}* transformants was measured by HPLC (Figure 6B). Analysis was restricted to the T1 generation because most of the abnormal *35S:AK2^{rsp1}* plants failed to produce seed. Two biological replicates of Col tissue produced highly similar Thr values (37.9 ± 1.2 pmol/mg fresh weight), indicating that major differences could be detected by single measurements. Also, the effect of BASTA pretreatment was evaluated with a control transgenic line not expressing AK2. Thr content measured for this line without treatment was highly similar to Col wild type and decreased by ~25% after BASTA treatment. The Thr content of *35S:AK2* transformants ranged between 13 and 32 pmol/mg (Figure 6B). Similar values were obtained from the phenotypically normal *35S:AK2^{rsp1}* transformants. By contrast, massive accumulation of Thr was detected in the *rsp1*-like transformants, rising to ~150-fold higher Thr content than the wild type. When *35S:AK2* and *35S:AK2^{rsp1}* T1 plants were inoculated with *Hpa* Noco2, pathogen sporulation was observed on all plants except *rsp1*-like *35S:AK2^{rsp1}* transformants included in the experiment, consistent with loss of susceptibility caused by *AK2^{rsp1}*. The increased accumulation of Lys, Thr, Ile, and Met in *rsp1* (Figure 5), the reduced Lys sensitivity of recombinant AK2^{rsp1} protein (Figure 6A), and the high Thr content of 35S:AK2^{rsp1} transformants phenotypically resembling the original *rsp1* mutant lead us to conclude that *rsp1* is a loss-of-inhibition allele of *AK2*. *rsp1* was therefore renamed *AK2^{rsp1}* to differentiate it from LOF alleles.

AK2^{rsp1} and *rsp2*/*dhdps2-2* Impede *Hpa* at an Early Stage of Infection

Having identified the molecular lesions underlying the *rsp* mutant phenotypes, we isolated single *AK2^{rsp1}* and *rsp2*/*dhdps2-2* mutants to characterize their impact on *Hpa* infection in a *RAR1* background with a fully functioning innate immune system. When infected with virulent *Hpa* Cala2, the *rsp* single mutants exhibited similar levels of resistance as the corresponding *rsp rar1-13* double mutant combinations (see Supplemental Figure 7 online), confirming that the *rsp* phenotype manifests independently of the *RAR1* status. We examined early stages of *Hpa* Cala2 infection (24 h after inoculation) by staining oomycete structures on the leaf surface with the optical brightener calcofluor. At this time point, germinating and fully germinated spores were visible on L*er* wild-type leaves, although the germination rate was low (~1%). Spore germination on *rsp1* leaves was indistinguishable from the wild type. By contrast, the germination rate appeared lower on *rsp2*, and we rarely located a germinating spore. This result suggested that *Hpa* colonization is impeded at a very early time point in *rsp2*. We then examined infection sites in the first pair of true leaves of wild-type and *rsp* mutant plants at 48 h after inoculation with Cala2 by TB staining. In the genetically resistant accession Col (due to *RPP2* recognition; Sinapidou et al., 2004), each infection site was associated with host cell death and there was no hyphal extension from these sites (Figure 7A). In susceptible L*er* wild type, 75% of primary infection sites produced hyphal outgrowth and no host cell death (Figure 7A). In *AK2^{rsp1}* and *rsp2*/*dhdps2-2* mutant leaves, the proportion of infection

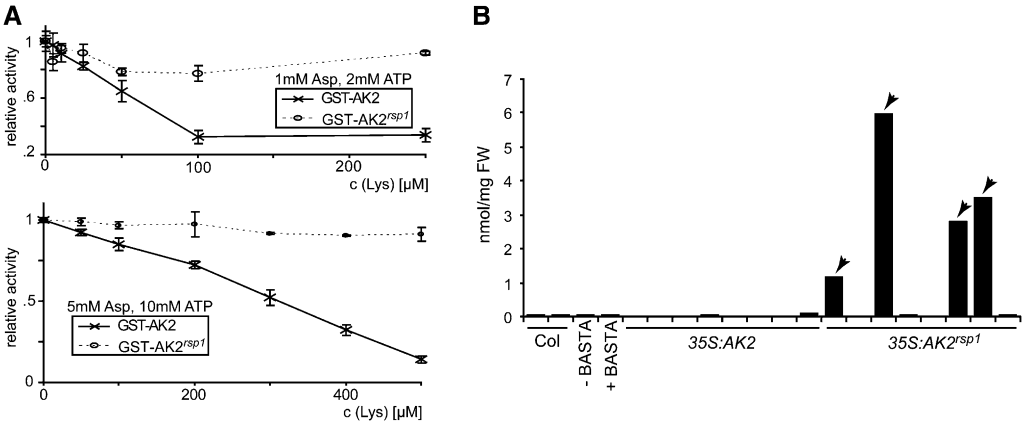

Figure 6. *rsp1* Is a Loss-of-Inhibition Allele of *AK2*.

(A) Asp kinase activity was assayed with wild-type (AK2) and mutant (AK2^{rsp1}) proteins using equal GST fusion protein amounts for enzymatic reactions in the presence of 1 mM Asp and 2 mM ATP (top panel) or 5 mM Asp and 10 mM ATP (bottom panel). Different concentrations of Lys were added to the reactions as indicated, and activity is expressed as percentage of activity without inhibitor. Standard deviations originating from four replicates are shown.

(B) Thr measurements from aerial tissue of *AK2* and *AK2*^{rsp1}-overexpressing plants. Transgenic plants were selected by BASTA resistance and confirmed by PCR. Leaf tissue was harvested from 5-week-old plants and used to determine free Thr content. Measurements derived from plants phenotypically resembling the *rsp1* mutant (see Supplemental Figure 6 online) are marked with arrowheads. As the fresh weight of these plants was not sufficient to perform replicate measurements, one single measurement was performed per plant. FW, fresh weight.

sites producing hyphal outgrowth reduced to 16 and 5%, respectively, but at no site was this associated with host cell death. Therefore, the reduced susceptibility of *AK2*^{rsp1} and *rsp2*/*dhdps2-2* mutants to *Hpa* infection is not due to activation of a classical resistance response. We found that *Hpa* could grow and form conidiophores at a low level on cotelydons of *AK2*^{rsp1} and *rsp2*/*dhdps2-2* and occasionally on true leaves of *AK2*^{rsp1} plants (Figure 7B). These phenotypes are in line with a metabolic imbalance or nutrient deficiency in the host-limiting early *Hpa* colonization of tissues.

The reduced growth of *rsp* mutant plants could be partially complemented on synthetic media by addition of Suc but not other osmolytes or signaling sugars to the media (see Supplemental Figures 8A and 8B online). Since this suggested that the *rsp* mutants might be limited for carbohydrate, we tested whether Suc could also restore susceptibility of *rsp* mutant plants to *Hpa*. Plants were initially grown on synthetic media containing Suc and were then transferred to soil at different time points before infection with *Hpa* and infections monitored by TB staining. Transfer of plants prior to infection increased disease susceptibility of wild-type and *rsp* mutant plants to a similar extent (see Supplemental Figure 8C online). Nutrient or carbohydrate deficiency is therefore unlikely to underlie *rsp* resistance to *Hpa*.

Testing of Candidate Metabolites for Resistance Induction in *rsp* Mutants

We reasoned that imbalances within the Lys superpathway might lead to increased production of secondary metabolites with resistance properties. For example, camalexin and indolic glucosinolates derived from Trp are important for resistance to adapted and nonadapted fungi (Bednarek et al., 2009, and references therein) and the hemibiotrophic oomycete pathogen *Phytophthora brassicae* (Schlaeppi et al., 2010). We measured levels of indole-derived secondary metabolites in wild-type and *rsp* mutant leaves. There were no differences in accumulation of the phytoalexin camalexin, but two- to threefold increased 1-methoxyindol-3-ylmethylglucosinolate levels were detected in *rsp1* and *rsp2* mutant extracts (see Supplemental Figure 10 online). We therefore tested the importance of indolic secondary metabolites in *Hpa* resistance by infecting *cyp79B2 cyp79B3* (*B2B3*) double mutant plants that are unable to convert Trp to indol-3-aldoxime (Zhao et al., 2002), which is the precursor of indolic secondary metabolites in *Arabidopsis*. Compared with wild-type Col, the *B2B3* mutant supported lower sporulation of virulent *Hpa* isolate Noco2 (Figure 8A), suggesting that indolic compounds do not contribute to *Arabidopsis* resistance to *Hpa*.

Both *rsp1* and *rsp2* accumulate high levels of Met, which is the precursor of *S*-adenosylmethionine, polyamines, ethylene, and aliphatic glucosinolates (Figure 5A). To test whether high Met content, either directly or through increased production of downstream metabolites, might contribute to resistance in the *rsp* mutants, we measured *Hpa* sporulation on *mto1-1* mutant plants carrying a mutation in a gene encoding cystathionine γ-synthase (Figure 5A), which leads to high Met accumulation (Inaba et al., 1994; Chiba et al., 1999). The *mto1-1* mutant plants supported similar levels of *Hpa* sporulation as the wild type (Figure 8B). Therefore, increased Met and its downstream metabolites do not explain the resistance in *rsp1* and *rsp2*.

rsp1 and *rsp2* also accumulate high levels of Thr and Ile. *Arabidopsis* mutants with increased levels of Thr and/or Ile in aerial tissue have been reported (Kim and Leustek, 2000; Garcia and Mourad, 2004), but these were unobtainable. Therefore, we

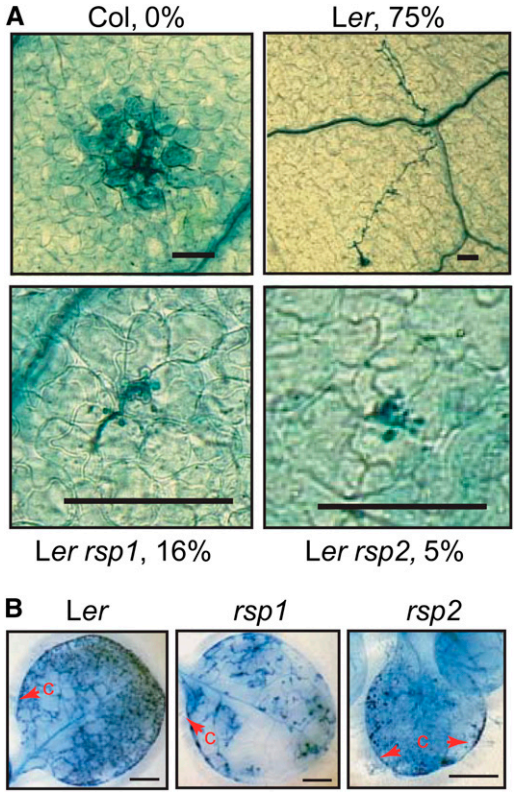

Figure 7. *rsp* Mutants Do Not Have Hallmarks of Active Resistance to *Hpa*.

(A) Successful *Hpa* hyphal outgrowth is reduced in *rsp* mutants. Three-week-old plants were infected with *Hpa* Cala2. First true leaves were stained with TB at 48 h after inoculation. Infection sites were analyzed and the fraction of sites with significant hyphal growth expressed as percentage of total infection sites. A representative picture of the predominant reaction is shown for each line. An HR is visible at the interaction site for resistant accession Col. At least 12 leaves were analyzed per genotype, and between 21 (*rsp2*) and 88 (*rsp1*) infection sites were evaluated for successful hyphal outgrowth and the occurrence of cell death. Additional pictures of infection structures for comparison of hyphal and haustorial morphologies are shown in Supplemental Figure 9 online. Bars = 62 μm.

(B) *Hpa* can grow and reproduce on *rsp* mutant plants. Infections were done as in **(A)** except TB stainings were performed at 7 d after inoculation on complete plants. Conidiophores (c) are marked with red arrowheads. True leaves are shown for L*er* and *rsp1*, and a cotelydon is shown for *rsp2*. Bars = 1 mm.

spray applied amino acid solutions onto hypersusceptible L*er eds1-2* plants to mimic the mutant metabolic state prior to infection with *Hpa* Cala2. HS was included in these experiments as induction of resistance to *Hpa* by this metabolite was recently reported (van Damme et al., 2009). Pretreatment of plants with Ile did not alter *Hpa* sporulation (Figure 8C). By contrast, sporulation was significantly reduced after HS and, to a stronger extent, Thr pretreatment. We detected only minor HS increases in *rsp* mutant tissues (see Supplemental Figure 11 online), suggesting that Thr accumulation is more likely to be causal for reduced *Hpa* growth on *rsp* mutant plants. Notably, suppression of *Hpa* growth by Thr application occurred in a dose-dependent manner (see Supplemental Figure 12 online).

Although our experiments indicate that indolic glucosinolates themselves are unlikely to contribute to *Hpa* resistance (Figure 8A), we examined whether jasmonate (JA)-regulated defenses

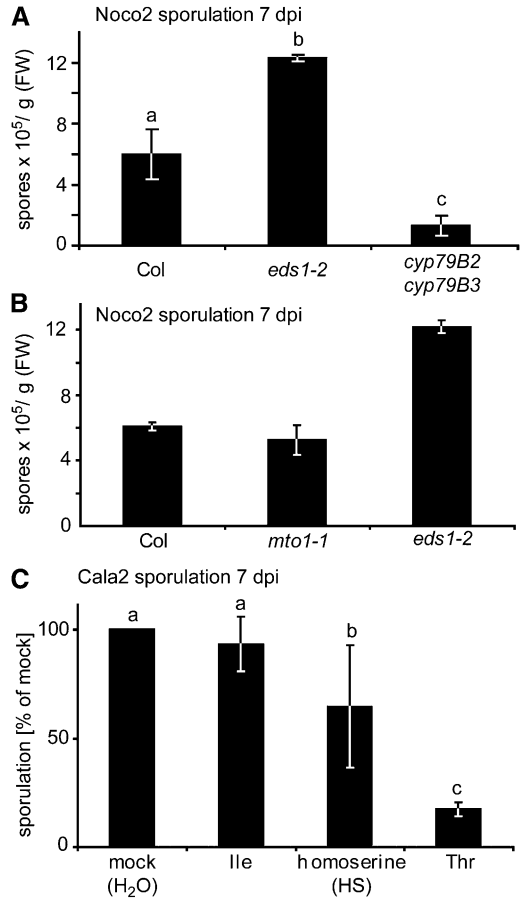

Figure 8. Thr and HS but Not Indolic Metabolites or Met-Derived Metabolites Affect *Arabidopsis* Susceptibility to *Hpa*.

(A) *cyp79B2 cyp79B3* double mutant plants are not hypersusceptible to *Hpa*. Three-week-old plants of the indicated genotypes were infected with *Hpa* isolate Noco2, and conidiospore formation was quantified at 7 d after inoculation. Error bars indicate standard deviations of three independent samples, and letters indicate significant differences (one-way ANOVA, Tukey's post-hoc test, $P < 0.05$ each). FW, fresh weight.

(B) Met or Met-derived metabolites do not confer *Hpa* resistance. Experiment was performed as in **(A)**. Biological replicates were pooled and treated as one sample. Error bars indicate technical error derived from five counts.

(C) Exogeneous Thr or HS treatments reduce *Hpa* conidiospore formation. Three-week-old L*er eds1-2* plants were sprayed with 5 mM solutions of the indicated amino acids 3 d and 1 d prior to infection with *Hpa* isolate Cala2. Conidiospores were quantified at 7 d after inoculation. Data were normalized to the mock-treated control (set at 100%) for seven independent biological replicates, and standard deviations are indicated. Significantly different classes are indicated by lower-case letters (one-way ANOVA, Tukey's post-hoc test, $P < 0.05$ each).

might underlie the *rsp* mutant phenotypes since JA application is known to induce indolic glucosinolate metabolites (Mikkelsen et al., 2003). The expression of JA marker genes was not significantly different between wild-type and *rsp* mutant tissues, and Thr application induced resistance to *Hpa* to the same extent in plants defective for JA biosynthesis or signaling (see Supplemental Figure 13 online). Therefore, JA-mediated defenses are not responsible for Thr-induced suppression of *Hpa* infection.

Thr Treatment Recapitulates *rsp* Mutant Resistance Phenotypes

Suppression of *Hpa* growth by Thr application might result from general toxicity of this metabolite and thus be unrelated to the *rsp* mutant phenotypes. To exclude this possibility, the same set of plants pretreated with Thr was infected with *Hpa* or *Go*. Col plants were used for this assay because *Go* sporulation was most uniform on this accession. Leaves from plants infected with virulent *Hpa* isolate Noco2 were stained with TB and examined under the microscope at 7 d after inoculation. *Hpa* growth was observed in all mock-treated leaves but not in Thr pretreated leaves (Figure 9A, left panel). By contrast, similar levels of *Go* sporulation were observed on mock- and Thr-treated plants (Figure 9A, right panel). Selective suppression of *Hpa* growth observed with the *rsp* mutants can therefore be reproduced by Thr application, excluding broad toxicity of Thr in the chemical treatment experiments.

We then tested whether Thr indeed accumulates in plant tissues after application. Since spray application would not allow us to discriminate between absorbed and surface-deposited Thr, we grew plants on synthetic media containing different concentrations of Thr and measured Thr accumulation in aerial tissues that were not in direct contact with the metabolite. We found that the *Hpa* infection-suppressing action of Thr could be reproduced under these conditions. L*er eds1-2* plants grown on Murashige and Skoog medium in the presence of 0 to 1.5 mM Thr were infected with *Hpa* Cala2 and symptom formation scored at 6 d after inoculation. The numbers of conidiophores produced diminished with increasing concentrations of Thr added to the medium (Figure 9B). Thr accumulation was measured by HPLC. Whereas aerial tissues of control plants contained ~0.3 nmol/mg (fresh weight) Thr, this increased to ~3 nmol/mg in tissues grown on 1 mM Thr (Figure 9C, left graph). We concluded that Thr accumulation in aerial tissue upon spray treatment is therefore highly likely. As inclusion of 1 mM Thr to the medium strongly suppressed *Hpa* infection in the plate assay, we analyzed the extent to which the Thr amounts measured under these conditions relate to *rsp* mutant Thr contents. Because *rsp* mutant plants cannot be cultivated on synthetic media lacking Suc (see Supplemental Figure 8 online) leaf samples of soil-grown *rsp* mutant and control plants were included in the HPLC analysis (Figure 9C, right graph). Thr amounts were similar in the in vitro– and soil-grown control plants, ranging from 0.33 to 0.36 nmol/mg, respectively (Figure 9C). Notably, Thr accumulation in aerial tissues of plants grown on media containing 1 mM Thr was comparable to levels found in *rsp* mutant tissues (ranging from 3.1 to 3.4 nmol/mg; Figure 9C). Altogether, the results suggest that Thr application closely mirrors the *rsp* mutant phenotypes, both with regard to Thr accumulation and suppression of *Hpa* infection.

Effects of Thr on Plant and *Hpa* Growth Correlate with Deployment of the Diaminopimelate Pathway

Thr toxicity for *Arabidopsis* grown in vitro has been described (Sarrobert et al., 2000), and expression of an *E. coli* Thr synthase in *Arabidopsis* produced Thr overaccumulating plants with wrinkled and thickened rosette leaves and infertility (Lee et al., 2005), phenotypes broadly resembling the *rsp1* and *rsp2* mutants and *AK2*^{rsp1} transgenic plants (see Supplemental Figures 1, 2, and 6 online). Also, lethality of *tha2-1* mutant plants defective in THREONINE ALDOLASE2, one of two *Arabidopsis* enzymes converting Thr to Gly, can be rescued by expression of *omr1-5*, a feedback-insensitive Thr deaminase (Figure 5A; Garcia and Mourad, 2004; Joshi et al., 2006), suggesting that *tha2-1* lethality is due to Thr toxicity (Joshi et al., 2006). Thr overaccumulation therefore appears to be detrimental to *Arabidopsis*. The *Hpa* infection phenotypes of *rsp* mutants (Figure 1) and chemical treatment results (Figure 9) point to a negative effect of Thr on *Hpa* but not *Go* infection. We reasoned that the target of Thr interference or a biosynthetic pathway negatively affected by high Thr accumulation might be conserved among plants and oomycetes but not in the fungal ascomycete *Go*. The presence of genes for biosynthesis of the amino acids Lys, Thr, and Met was therefore compared in a targeted manner between the three different phyla. Thr and Met are derived from Asp in all organisms and their biosynthesis appears to be broadly similar. Ascomycetes use the α-aminoadipate (AAA) pathway with α-ketoglutarate serving as a precursor for biosynthesis of Lys, which thus belongs to the Glu family of amino acids (reviewed in Xu et al., 2006). By contrast, Lys is produced through the diaminopimelate (DAP) pathway in plants and oomycetes and belongs to the Asp family (Figure 5A; Randall et al., 2005; Hudson et al., 2006).

In order to test for deployment of the DAP pathway by *Hpa*, homologs of DHDPS, dihydrodipicolinate reductase (DHDPR), and diaminopimelate decarboxylase (LysA), which are common to all types of DAP pathway, were searched for in the newly available *Hpa* genome (see Supplemental Table 1 online; Baxter et al., 2010). Sequences with high similarity to *E. coli* DHDPS and LysA were detected. For DHDPR, a sequence with moderate similarity to *E. coli* DapB was found. Notably, the Pfam DHDPR N-terminal (PF01113) and C-terminal (PF05173) domains were identified in the predicted *Hpa* DHDPR protein. The presence of all three marker genes suggests that Lys biosynthesis occurs via the DAP pathway in *Hpa*. No sequences supporting the presence of these enzymes were obtained when searching the *Go* and related *Blumeria graminis* (*Bg*) genome assemblies (Spanu et al., 2010). By contrast, there was strong evidence for the presence of the AAA pathway in *Go* and *Bg* (see Supplemental Table 1 online). Sequences similar to genes of the AAA pathway were also detected in *Hpa*. Reciprocal sequence comparisons generally revealed higher similarity to proteins of different function, as previously described for *Phytophthora infestans* (Randall et al., 2005), arguing against co-option of both DAP and AAA pathways for Lys biosynthesis in oomycetes. We concluded that detrimental effects of Thr on *Arabidopsis* growth and *Hpa* infection likely

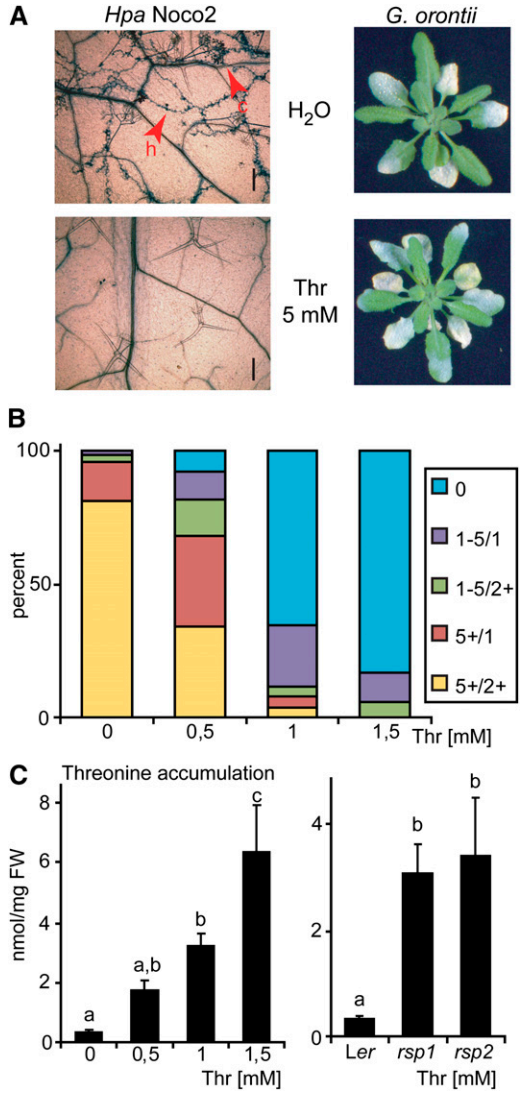

Figure 9. Thr Treatment Mimics *rsp* Mutant Phenotypes.

(A) Thr treatment induces resistance to *Hpa* but not *Go*. Four-week-old Col plants were spray treated with Thr as described (Figure 8C). Plants were then infected with either *Hpa* (isolate Noco2) or *Go*. Disease symptom formation was evaluated macroscopically at 7 d after inoculation (*Go* infection) or assessed microscopically after TB staining (*Hpa* infection). Additional pictures to display the spectrum of pathogen growth are shown in Supplemental Figure 14 online. h, hyphae; c, conidiophores. Bars = 0.2 mm.

(B) Growth of plants on media containing Thr suppresses *Hpa* growth. Three-week-old L*er eds1-2* plants grown on synthetic media containing different concentrations of Thr were infected with *Hpa* isolate Cala2. Conidiophore formation was assessed 6 d after inoculation and categorized: 0, no conidiophores; 1-5/1, one to five conidiophores on one leaf; 1-5/2+, one to five conidiophores on two or more leaves; 5+/1, more than five conidiophores on one leaf; 5+/2+, more than five conidiophores on two or more leaves; $n \geq 18$. Similar results were obtained in three independent experiments.

(C) Thr accumulation in *rsp* mutant tissues and plants grown on media containing *Thr*. Plants from **(B)** were sampled prior to infection and Thr content measured by HPLC (left graph) in parallel with samples from soil-grown *rsp* mutant plants (right graph). Data from **(B)** and **(C)** are derived from the same experiment. HPLC measurements were performed with ≥4 biological replicates. Significantly different classes are indicated by lower-case letters (one-way ANOVA, Tukey's post-hoc test, $P < 0.05$ each). FW, fresh weight.

reflect operation of a complex and highly regulated DAP pathway in both systems.

DISCUSSION

Obligate biotrophy implies strong interdependence between host metabolism and nutrient uptake by the pathogen, but the processes allowing establishment and maintenance of a compatible interaction are poorly understood. Here, we show that the primary amino acid metabolic status of a plant can profoundly affect its suitability as an infection substrate for the adapted obligate biotrophic oomycete pathogen, *Hpa*.

The *rsp2* LOF mutant carries a lesion in DHDPS2 (Figure 3), one of two *Arabidopsis* DHDPS enzymes catalyzing the conversion of ASA to L-2,3-dihydrodipicolinate as the committing step in Lys biosynthesis (Figure 5A). Although expression of *DHDPS2* in *Arabidopsis* was initially reported to be restricted to the root tip (Sarrobert et al., 2000) and mainly vascular tissue in aerial parts (Craciun et al., 2000), analysis of public microarray data (http://www.genevestigator.com) suggests similar levels of *DHDPS2* expression in roots and rosette leaves, both of which are colonized by *Hpa* (Coates and Beynon, 2010). *DHDPS1* has a similar expression pattern but with lower overall signal intensity according to microarray data. Since *dhdps1* mutant plants did not exhibit altered growth or pathogen resistance (see Supplemental Figure 3 online), DHDPS2 probably accounts for the main DHDPS activity in *Arabidopsis*. We did not attempt to generate double mutants, as these would be expected to be lethal because no alternative route for Lys biosynthesis is known. Both DHDPS and HSDH, which catalyzes the committing step toward the biosynthesis of Met, Thr, and Ile, use ASA as a common substrate. Due to flux partitioning at the DHDPS/HSDH node, loss of the major DHDPS isoform leads to increased accumulation of products of the Met, Thr, and Ile branch (Figure 5). As Lys is a key regulator of Asp kinases (Curien et al., 2007), flux into the entire pathway is likely increased through compensatory control to reestablish Lys accumulation (for a kinetic model of the pathway, see Curien et al., 2009).

The *rsp1* mutation isolated in our study perturbs the Lys superpathway in a different manner to *rsp2*/*dhdps2-2*. We show that *rsp1* is a loss-of-inhibition allele of *AK2*, which renders the mutant AK2^{rsp1} protein refractive to allosteric inhibition by Lys under physiological conditions (Figures 4 and 6). Allosteric transitions deduced from the structures of *E. coli* AKIII suggest that subtle interdomain movements at the dimer interface are involved in the R- to T-state transition (Kotaka et al., 2006). The exchange of Val-430 located in the dimer interface to Met in AK2^{rsp1} might impede state transition or directly interfere with inhibitor binding. This molecular characterization of a feedback-insensitive AK variant from *Arabidopsis* adds to knowledge

gained by prior isolation of presumed *aspartate kinase* mutants with altered regulatory properties (Heremans and Jacobs, 1997). Consistent with a failure in feedback inhibition, expression of AK2^{rsp1} from its endogenous locus increases flux into the Lys superpathway leading to accumulation of all pathway end products (Figure 5B).

AK2 and *DHDPS2* were not obviously linked to plant immunity. This is probably because mutations in these genes do not lead to broad spectrum resistance (Figure 2) but appear to specifically impede colonization by *Hpa*. Basal innate immunity to adapted *Hpa* isolates is normally mediated by SA-dependent processes and numerous mutants with constitutively induced SA defenses display enhanced resistance to *Hpa* (Lu et al., 2003; Zhang et al., 2003). In contrast with these mutants, neither *rsp1* nor *rsp2* has characteristics of primed or constitutive SA pathway activation (Figure 2). Importantly, in an immune-competent wild-type background, *rsp1* and *rsp2* suppressed colonization by virulent *Hpa* isolate Cala2 at an early stage of infection, although the sporadic microcolonies formed in *rsp1* did eventually grow and produce some spores (Figure 7). None of the successful or unsuccessful infection sites were associated with host cell death in the *rsp* mutants. Therefore, the reduced *Hpa* growth on *rsp1* and *rsp2* leaves is not through activation of a classical immune response but rather due to a loss of susceptibility. We conclude that perturbations in host metabolism render tissues unsuitable as an *Hpa* infection substrate.

We performed a number of experiments to elucidate how the host metabolic status might interfere with *Hpa* infection. While provision of Suc partially restored *rsp* mutant plant growth in vitro, scarcity of carbohydrates is unlikely to underlie the reduced susceptibility of *rsp1* and *rsp2* plants because *Hpa* growth was not appreciably restored by Suc (see Supplemental Figure 8 online). Suppression of *Hpa* growth through increased accumulation of indolic glucosinolates or Met-derived compounds is also not supported by our data (Figure 8; see Supplemental Figure 10 online). In chemical application experiments, we identified Thr as a potent inhibitor of *Hpa* growth (Figure 8C). Indeed, the consequences of Thr application compare well with *rsp* mutant phenotypes both with regard to selective suppression of *Hpa* growth and to absolute Thr concentrations (Figure 9). It is possible that a toxic metabolite derived from or induced by Thr accumulates upon increased Thr abundance. Since neither *rsp* mutant metabolic state nor Thr application interfered with growth of the adapted biotrophic ascomycete *Go* (Figure 9A; see Supplemental Figure 2 online), such a metabolite would have to act specifically on *Arabidopsis* and *Hpa*, but not *Go*. Alternatively, Thr itself could interfere with host and pathogen biosynthetic pathways. Negative effects of Thr by feedback inhibition of the Lys superpathway have been proposed, although failure to rescue lethality of *tha2-1* mutant plants accumulating excess Thr by amino acid supplementation suggests otherwise (Joshi et al., 2006). Similarly, we could not restore *Hpa* growth on *rsp* mutant plants by providing an amino acid solution upon infection. Surprisingly, however, we also could not rescue the poor growth of the *rsp2*/*dhdps2-2* mutant by Lys supplementation of synthetic media lacking Suc. This suggests an unexpected degree of compartmentalization or additional regulatory mechanisms operating within the Lys superpathway. The precise molecular processes underlying Thr interference remain to be elucidated. We think it likely that Thr overaccumulation interferes with both host and oomycete metabolic processes due to the relatively close phylogeny of the two organisms and the deployment of the DAP pathway in contrast with the more distant ascomycete *Go* (see Supplemental Table 1 online; Burki et al., 2007).

Two additional loci, *AGD2* and *DMR1*, encoding enzymes of the Lys superpathway have previously been described as having effects on plant immune responses. AGD2 was shown to be a LL-diaminopimelate decarboxylase catalyzing the last step of Lys biosynthesis (Figure 5A; Hudson et al., 2006), and *agd2* mutant plants exhibited increased resistance to bacteria and *Hpa* (Song et al., 2004). We measured the amino acid content of *agd2* and detected an approximately twofold increase in Thr content (see Supplemental Figure 15 online), supporting relevance to Lys biosynthesis in vivo. While this small increase in Thr content might contribute to *agd2 Hpa* resistance, the mutant does not resemble *rsp1* and *rsp2* since it displays constitutive resistance (Song et al., 2004). By contrast, *dmr1* mutant plants defective in homoserine kinase were resistant to *Hpa* without the hallmarks of constitutive resistance (van Damme et al., 2009). The similar phenotypes of three independent mutants (*rsp1*, *rsp2*, and *dmr1*) affected in enzymes of the Lys superpathway point to a common mechanism leading to impairment of *Hpa* infection. Our data support Thr as being causal for *Hpa* growth suppression in *rsp* mutant tissues, whereas *dmr1* mutant plants preferentially accumulate HS (van Damme et al., 2009). It is conceivable that HS taken up by *Hpa* is subsequently converted to Thr, which might then accumulate in *Hpa* tissues. In *Arabidopsis*, HS is rate limiting for the accumulation of downstream metabolites under normal conditions and HS supplementation leads to Thr accumulation (Lee et al., 2005). Genes encoding enzymes of the initial and final reactions of Thr, Ile, and Met biosynthesis and for putative amino acid transporters/permeases are present in *Hpa* according to primary transcript annotations (http://vmd.vbi.vt.edu/query.php). Also, van Damme et al. (2009) showed HS-induced *Hpa* growth suppression to be independent from known defense pathways. These data lend support to our hypothesis that incompatibility with *Hpa* arises by an imbalance in amino acid homeostasis. Here, characterization of the *Arabidopsis rsp1* and *rsp2* mutants provides a new insight to how plant metabolic status can selectively determine interactions with pathogens. It also prompts a deeper comparative analysis of biotrophic pathogen metabolite uptake and assimilation systems that may also influence host plant selection.

METHODS

Plant Material, Growth Conditions, and Pathogenicity Assays

Wild-type *Arabidopsis thaliana* accessions used were Col-0 and L*er*. The L*er rar1-13*, *rar1-15* (Muskett et al., 2002), *eds1-2* (Aarts et al., 1998), and Col *mlo2-6* (Consonni et al., 2006), *mto1-1* (Inaba et al., 1994), and *cyp79B2 cyp79B3* (Zhao et al., 2002) mutants are published. Col *dhdps1-1* (SALK_147470), *dhdps2-3* (GABI-KAT_180F08) (Rosso et al., 2003), *ak2-1* (SAIL_258_E06, Syngenta), L*er rsp2*/*dhdps2-2*, and *rsp1*/*AK2*^{rsp1} are characterized here. Oligonucleotides used for genotyping are listed in Supplemental Table 2 online. Plants were grown in soil in controlled environment chambers under a 10-h light regime (150 to 200 $\mu E/m^2s$) at

22°C and 65% relative humidity. Plants were grown in vitro on one-tenth Murashige and Skoog medium, optionally containing different sugars or amino acids, under long-day conditions (18 h light) at 21°C. *Pst* DC3000 bacteria were grown for 24 h at 28°C on solid NYG medium (0.5% peptone, 0.3% yeast extract, and 2% glycerol) supplemented with the corresponding antibiotics. For bacterial growth assays, 6-week-old plants were spray inoculated with bacterial suspensions at 4×10^8 colony-forming units/mL in 10 mM $MgCl_2$ containing 0.04% (v/v) Silwet L-77 (Lehle Seeds). In planta bacterial titers were determined at the indicated time points as described (Tornero and Dangl, 2001). *Hpa* isolates Noco2 and Cala2 were inoculated onto 3-week-old plants at 4×10^4 spores/mL unless indicated otherwise. Plant cell death and *Hpa* infection structures were visualized under a light microscope after staining leaves with lactophenol TB as described (Muskett et al., 2002) or directly using binocular UV illumination and a GFP1 filter. For quantitative assays, three pots of each genotype were infected and treated as biological replicates. Plants were harvested 6 to 7 d after inoculation and their fresh weight determined, and spores were resuspended in 5 to 10 mL of water and spore concentrations counted using a Neubauer counting chamber under the microscope. For *Go* inoculations, 4- to 6-week-old plants (as indicated) were touch infected with leaves of sporulating host plants. Host entry rate was determined 2 d after inoculation after destaining leaves with ethanol/acetic acid and staining fungal structures with Coomassie Brilliant Blue. Germinating spores with secondary hyphae were considered as having successfully penetrated.

Expression Analyses

Plants were spray infected with *Hpa* Noco2 as described above, and leaf samples (~50 mg) from different plants were taken at the indicated time points. Total RNA was extracted from leaves using TRI reagent (Sigma-Aldrich), and RNA was reverse transcribed into cDNA using SuperScriptII (Invitrogen) following the manufacturer's instructions. Quantitative RT-PCR experiments were performed in an iQ5 Real-Time PCR detection system (Bio-Rad) using Brilliant SYBR Green QPCR Core Reagent (Stratagene) as dye. Experiments were performed using three independent biological samples. Relative transcript levels were calculated using the iQ5 Optical System Software (version 2.0). *Ubiquitin UBQ10* (At4g05320) transcript levels were used as internal reference. Primers used are listed in Supplemental Table 2 online.

GC-MS Analyses

SA quantification was done as previously described (Straus et al., 2010). For amino acid analysis, metabolites were extracted from 100 mg ground leaf tissue in 1 mL $CHCl_3$/CH_3OH/water (1:2:0.3). After shaking for 10 min at 70°C, samples were centrifuged and reextracted with 500 μL $CHCl_3$/CH_3OH (2:1). Five hundred microliter of water was added to the pooled supernatants, which were then centrifuged for phase separation. The upper phase was collected and dried. To separate polar from semipolar metabolites, the dried extract was resuspended in 0.5 mL of water with 0.1% trifluoroacetic acid and loaded onto a 100 mg DCS-18 solid phase extraction column (Supelco). Columns were washed twice with 0.6 mL of water containing 0.1% trifluoroacetic acid. For analysis of polar metabolites, the flow-through and washes were collected, dried, and resuspended in 400 μL CH_3OH. A 100-μL aliquot was dried and derivatized in 40 μL *N*-methyl-*N*-(trimethylsilyl)trifluoroacetamide with 1% trimethylchlorosilane (Fluka) and 40 μL pyridine, including a mix of fatty acid methyl ester (Sigma-Aldrich) as internal standards for 30 min at 90°C. One microliter was injected into a GC-MS system equipped with a HP-5MS column (Agilent). Amino acids were identified by running commercial standards under the same conditions and quantified with Chemstation software from Agilent.

HPLC Analysis

Analysis of indolic glucosinolates was performed as previously described (Bednarek et al., 2009). For amino acid analyses, 100 mg leaf material were used for extractions if available, but less tissue was used for severely affected *35S:AK2^{rsp1}* transgenic plants. Free amino acids were determined using a modified protocol from Scheible et al. (1997). Plant material was extracted for 20 min at 4°C with 400 μL 80% (v/v) aqueous ethanol (2.5 mM HEPES-KOH, pH 7.5) and 400 μL 50% (v/v) aqueous ethanol (2.5 mM HEPES-KOH, pH 7.5) and then 200 μL 80% (v/v) aqueous ethanol. Amino acids were measured in the collected supernantants by precolumn derivatization with orthophthaldehyde in combination with fluorescence detection (λex 330/λem 450) as described (Kreft et al., 2003). Elution was achieved on a Hyperclone C18 BDS column (Phenomenex) on a Summit HPLC system (Dionex), applying a solvent gradient with increasing hydrophobicity (buffer A: 0.2% [v/v] THF, 8.5 mM sodium phosphate buffer [NAPI], pH 7.5; buffer B: 32.5% [v/v] methanol, 20.5% [v/v] acetonitrile, and 18.5 mM NAPI, pH 7.5; flow: 0.8 mL/min; 0 to 2 min: 100% A, 16 min: 77% A, 13% B; 23.25 min: 15% A, 85% B; 32.23 min: 50% A, 50% B; 43.30 min: 40% A, 60% B; 49 to 52 min 100% B, 53 to 60 min: 100% A).

Protein Alignments and Modeling

Protein alignments were made using TCoffee (http://tcoffee.vital-it.ch/cgi-bin/Tcoffee/tcoffee_cgi/index.cgi) and graphical views generated with ESPript (http://espript.ibcp.fr/ESPript/ESPript/). Comparative modeling of the At AK2 structure was performed with the modeller9v3 program (Sali and Blundell, 1993) using the structure of At AK1 (PDB: 2CDQ) as template. The high sequence identity between At AK1 and At AK2 (77%) ensures that errors in the model should not exceed 1 Å in Cα root mean square deviation. Mutation $V_{375}M$ in each chain of the dimer At AK2 could be modeled using the backrub module of the rosettav2.3 program (Smith and Kortemme, 2008). Figures were generated using Pymol.

Stable Transgenic Lines

The AK2 coding region was amplified from cDNA and cloned into pENTR/D-TOPO (Invitrogen), and the *rsp1* mutation was introduced using site-directed mutagenesis by PCR with complementary oligonucleotides. Primers are listed in Supplemental Table 2 online. Wild-type and mutant AK2 sequences were recombined into Gateway-converted pAM-PAT-MCS. Plasmids were transformed into *Agrobacterium tumefaciens* strain GV3101:pMP90RK for transformation of *Arabidopsis* plants using the floral dip method (Logemann et al., 2006).

Recombinant Protein Expression and Purification

A cDNA sequence coding for AK2 with the initiating Met introduced at position 61 to remove the chloroplast targeting peptide was amplified by PCR and cloned into pENTR/D-TOPO, yielding pE AK2_STOP. The *rsp1* mutation was introduced by site-directed mutagenesis giving rise to pE AK2^{rsp1}_STOP. Sequences were recombined into pDEST15 (Invitrogen) and confirmed plasmids were transformed into *Escherichia coli* Rosetta (Novagen). For protein expression, bacteria were grown at 37°C in Luria-Bertani media to an OD_{600} of 0.6, and expression was then induced by addition of 1 mM isopropyl β-D-1-thiogalactopyranoside, and bacteria were grown for additional 16 h at 15°C. Bacteria were harvested by centrifugation, taken up in buffer A (50 mM Tris, pH 7.4, 50 mM KCl, 2 mM lysine, 2 mM DTT, 1 mM EDTA, and 10% glycerol) supplemented with Complete Protease inhibitor without EDTA (Roche), DNaseI, and Lysozyme, and lysed by sonification. Lysates were cleared by centrifugation (30 min, 4°C, 30,000*g*), filtered through 0.22-μm PES membrane filters

and batch incubated with 1 mL preequilibrated GST-Sepharose (GE Healthcare) for 1 h. Beads were transferred to 10-mL filter columns (Bio-Rad) and washed with buffer A, then with buffer A containing 300 mM NaCl and finally reequilibrated with buffer A. Proteins were eluted with buffer A containing 10 mM reduced glutathione, concentrated using Vivaspin devices (Sartorius), and buffer exchanged on a HiTrap column (GE Healthcare) equilibrated with buffer B (50 mM Tris, pH 7.4, 50 mM KCl, and 10% glycerol). Proteins were reconcentrated, aliquoted, and stored at −80°C. Purity was confirmed by SDS-PAGE followed by Coomassie Brilliant Blue staining and protein concentration determined by Bradford assay according to the manufacturer (Bio-Rad).

Asp Kinase Activity Assay

AK was assayed using the hydroxamate assay as previously described (Ferreira et al., 2006) with minor modifications. Forty microliters of reaction buffer (25 mM Tris, pH 7.4, 1 mM DTT, 5% glycerol, 2 mM ATP, 1 mM Asp, 10 mM $MgSO_4$, and 500 mM hydroxylamine) was made up to 50 μL with buffer B, proteins contained in buffer B, and/or buffer B containing Lys. After incubation at 35°C, 1 volume of STOP solution was added (0.67 M $FeCl_3$, 0.5 M HCl, and 20% [w/v] trichloractetic acid), and absorbance was measured at 490 nm. The assays were repeated with higher substrate concentrations (5 mM Asp and 10 mM ATP), as these conditions yielded more robust data.

Bioinformatic Analysis

The genomes of *Hpa* (gene models v8.3; http://vmd.vbi.vt.edu/), *Bg* (https://www.blugen.org/), and *Go* (local BLAST server) were queried for sequences with similarity to the sequences of enzymes of AAA and DAP pathway listed in Supplemental Table 1 online using TBLASTn with default settings. Returned sequences producing significant alignments ($E \leq$ 1e-5) were considered as possible presence of a gene, listed in Supplemental Table 1 online, and used for a reciprocal BLAST search. The first iteration of the PSI-BLAST algorithm (http://www.ebi.ac.uk/Tools/sss/psiblast/) was used with default settings against the UniProt Knowledgebase. From this reciprocal BLAST search, the first entry with an informative annotation was listed in Supplemental Table 1 online to support or not the results of first BLAST searches. Presence of a gene was concluded if an alignment with $E \leq$ 1e-35 was obtained in the first BLAST search. The result of the reciprocal BLAST was used as judgment for returned results with 1e-35 $\leq E \leq$ 1e-5.

Accession Numbers

Sequence data from this article can be found in the Arabidopsis Genome Initiative or GenBank/EMBL databases under the following accession numbers: *RAR1* (*At5g51700*), *EDS1* (*At3g48090*), *PR1* (*At2g14610*), *MLO2* (*At1g11310*), *DHDPS1* (*At3g60880*), *DHDPS2* (*At2g45440*), *AK2* (*At5g14060*), *PDF1.2* (*AT5G44420*), *VSP2* (*AT5G24770*), *OPR3* (*AT2G06050*), *JAR1* (*AT2G46370*), *JIN1* (*AT1G32640*), *AOS* (*AT5G42650*), *THA2* (*AT3G04520*), and *OMR1* (*AT3G10050*).

Supplemental Data

The following materials are available in the online version of this article.

Supplemental Figure 1. Phenotypes of *rar1-13 rsp1* and *rsp2* Double Mutants.

Supplemental Figure 2. Macroscopic Disease Symptom Formation upon *Golovinomyces orontii* Infection.

Supplemental Figure 3. Isolation and Characterization of a Col *dhdps1-1* Mutant.

Supplemental Figure 4. Germination Phenotype of *rsp* Mutants.

Supplemental Figure 5. Characterization of a Putative *ak2* Loss-of-Function Mutant.

Supplemental Figure 6. Macroscopic Phenotypes of T1 Plants Overexpressing Wild-Type AK2 or Mutant $AK2^{rsp1}$.

Supplemental Figure 7. *Hpa* Resistanceof *rsp* Mutants Is Not *rar1-13* Dependent.

Supplemental Figure 8. Effects of Sugar on Growth and *Hpa* Susceptibility of *rsp* Mutants.

Supplemental Figure 9. *Hpa* Infection Structures of Virulent *Hpa* Isolate Cala2 on *rsp1* and *rsp2* Mutant Plants.

Supplemental Figure 10. Indole Glucosinolate Content of *rsp* Mutant Plant Tissues.

Supplemental Figure 11. Homoserine Content of *rsp* Mutant Plants.

Supplemental Figure 12. Dose Dependency of *Hpa* Growth Suppression by Thr.

Supplemental Figure 13. Expression of JA-Regulated Genes in *rsp* Mutant Plants and Thr-Induced *Hpa* Growth Suppression on JA-Signaling Mutants.

Supplemental Figure 14. Growth of *Hpa* on Mock- or Threonine-Treated Col Plants.

Supplemental Figure 15. Threonine Content of *agd2* Mutant Tissues.

Supplemental Table 1. Comparative Genome Analysis for Genes Coding DAP/AAA Pathway Enzymes in *Hyaloperonospora arabidopsidis*, *Golovinomyces orontii*, and *Blumeria graminis*.

Supplemental Table 2. Oligonucleotides Used in This Study.

ACKNOWLEDGMENTS

We thank the Salk Institute Genomic Analysis Laboratory for providing the sequence-indexed *Arabidopsis* T-DNA insertion mutants and the Nottingham Arabidopsis Stock Centre for distribution of *Arabidopsis* lines. We thank G. Jander and P. Schulze-Lefert for helpful discussions, S. Lagauzere, D. Becker, and N. Moret for technical assistance, and Emiel Ver Loren van Themaat for help with bioinformatic analysis. We also thank L. Nussaume, J. Greenberg, G. Van den Ackerveken, R. Ros, and Y. Yoshioka for providing mutant *Arabidopsis* seed. This work was funded by the Max-Planck Society, Deutsche Forschungsgemeinshaft funding within Collaborative Research Centre (SFB) '635' (J.E.P. and J.S.), and Deutsche Forschungsgemeinshaft Grant PA 917/3-1 (J.E.P. and S.R.).

AUTHOR CONTRIBUTIONS

J.S. and J.E.P. designed research and wrote the article. J.S., S.R., J.K., P.M., and P.B. performed experiments and analyzed data. H.-M.H. and R.H. performed metabolite profiling. R.G. performed structural modeling and interpretation.

Received May 25, 2011; revised June 27, 2011; accepted July 7, 2011; published July 22, 2011.

REFERENCES

Aarts, N., Metz, M., Holub, E., Staskawicz, B.J., Daniels, M.J., and Parker, J.E. (1998). Different requirements for *EDS1* and *NDR1* by

disease resistance genes define at least two *R* gene-mediated signaling pathways in *Arabidopsis*. Proc. Natl. Acad. Sci. USA **95:** 10306–10311.

Baxter, L., et al. (2010). Signatures of adaptation to obligate biotrophy in the *Hyaloperonospora arabidopsidis* genome. Science **330:** 1549–1551.

Bednarek, P., Pislewska-Bednarek, M., Svatos, A., Schneider, B., Doubsky, J., Mansurova, M., Humphry, M., Consonni, C., Panstruga, R., Sanchez-Vallet, A., Molina, A., and Schulze-Lefert, P. (2009). A glucosinolate metabolism pathway in living plant cells mediates broad-spectrum antifungal defense. Science **323:** 101–106.

Bent, A.F., and Mackey, D. (2007). Elicitors, effectors, and *R* genes: The new paradigm and a lifetime supply of questions. Annu. Rev. Phytopathol. **45:** 399–436.

Burki, F., Shalchian-Tabrizi, K., Minge, M., Skjaeveland, A., Nikolaev, S.I., Jakobsen, K.S., and Pawlowski, J. (2007). Phylogenomics reshuffles the eukaryotic supergroups. PLoS ONE **2:** e790.

Büschges, R., et al. (1997). The barley *Mlo* gene: a novel control element of plant pathogen resistance. Cell **88:** 695–705.

Chiba, Y., Ishikawa, M., Kijima, F., Tyson, R.H., Kim, J., Yamamoto, A., Nambara, E., Leustek, T., Wallsgrove, R.M., and Naito, S. (1999). Evidence for autoregulation of cystathionine gamma-synthase mRNA stability in *Arabidopsis*. Science **286:** 1371–1374.

Coates, M.E., and Beynon, J.L. (2010). *Hyaloperonospora arabidopsidis* as a pathogen model. Annu. Rev. Phytopathol. **48:** 329–345.

Conrath, U., Pieterse, C.M., and Mauch-Mani, B. (2002). Priming in plant-pathogen interactions. Trends Plant Sci. **7:** 210–216.

Consonni, C., Humphry, M.E., Hartmann, H.A., Livaja, M., Durner, J., Westphal, L., Vogel, J., Lipka, V., Kemmerling, B., Schulze-Lefert, P., Somerville, S.C., and Panstruga, R. (2006). Conserved requirement for a plant host cell protein in powdery mildew pathogenesis. Nat. Genet. **38:** 716–720.

Craciun, A., Jacobs, M., and Vauterin, M. (2000). *Arabidopsis* loss-of-function mutant in the lysine pathway points out complex regulation mechanisms. FEBS Lett. **487:** 234–238.

Curien, G., Bastien, O., Robert-Genthon, M., Cornish-Bowden, A., Cárdenas, M.L., and Dumas, R. (2009). Understanding the regulation of aspartate metabolism using a model based on measured kinetic parameters. Mol. Syst. Biol. **5:** 271.

Curien, G., Laurencin, M., Robert-Genthon, M., and Dumas, R. (2007). Allosteric monofunctional aspartate kinases from *Arabidopsis*. FEBS J. **274:** 164–176.

Curien, G., Ravanel, S., Robert, M., and Dumas, R. (2005). Identification of six novel allosteric effectors of *Arabidopsis thaliana* aspartate kinase-homoserine dehydrogenase isoforms. Physiological context sets the specificity. J. Biol. Chem. **280:** 41178–41183.

Ferreira, R.R., Meinhardt, L.W., and Azevedo, R.A. (2006). Lysine and threonine biosynthesis in sorghum seeds: characterisation of aspartate kinase and homoserine dehydrogenase isoenzymes. Ann. Appl. Biol. **149:** 77–86.

Garcia, E.L., and Mourad, G.S. (2004). A site-directed mutagenesis interrogation of the carboxy-terminal end of *Arabidopsis thaliana* threonine dehydratase/deaminase reveals a synergistic interaction between two effector-binding sites and contributes to the development of a novel selectable marker. Plant Mol. Biol. **55:** 121–134.

Hakoyama, T., et al. (2009). Host plant genome overcomes the lack of a bacterial gene for symbiotic nitrogen fixation. Nature **462:** 514–517.

Heremans, B., and Jacobs, M. (1997). A mutant of *Arabidopsis thaliana* (L.) Heynh. with modified control of aspartate kinase by threonine. Biochem. Genet. **35:** 139–153.

Holub, E.B., Beynon, J.L., and Crute, I.R. (1994). Phenotypic and genotypic characterization of interactions between isolates of *Peronospora parasitica* and accessions of *Arabidopsis thaliana*. Mol. Plant Microbe Interact. **7:** 223–239.

Hudson, A.O., Singh, B.K., Leustek, T., and Gilvarg, C. (2006). An LL-diaminopimelate aminotransferase defines a novel variant of the lysine biosynthesis pathway in plants. Plant Physiol. **140:** 292–301.

Inaba, K., Fujiwara, T., Hayashi, H., Chino, M., Komeda, Y., and Naito, S. (1994). Isolation of an *Arabidopsis thaliana* mutant, *mto1*, that overaccumulates soluble methionine (temporal and spatial patterns of soluble methionine accumulation). Plant Physiol. **104:** 881–887.

Jander, G., and Joshi, V. (2010). Recent progress in deciphering the biosynthesis of aspartate-derived amino acids in plants. Mol. Plant **3:** 54–65.

Joshi, V., Laubengayer, K.M., Schauer, N., Fernie, A.R., and Jander, G. (2006). Two *Arabidopsis* threonine aldolases are nonredundant and compete with threonine deaminase for a common substrate pool. Plant Cell **18:** 3564–3575.

Kale, S.D., et al. (2010). External lipid PI3P mediates entry of eukaryotic pathogen effectors into plant and animal host cells. Cell **142:** 284–295.

Kämper, J., et al. (2006). Insights from the genome of the biotrophic fungal plant pathogen *Ustilago maydis*. Nature **444:** 97–101.

Kim, J., and Leustek, T. (2000). Repression of cystathionine γ-synthase in *Arabidopsis thaliana* produces partial methionine auxotrophy and developmental abnormalities. Plant Sci. **151:** 9–18.

Kotaka, M., Ren, J., Lockyer, M., Hawkins, A.R., and Stammers, D.K. (2006). Structures of R- and T-state *Escherichia coli* aspartokinase III. Mechanisms of the allosteric transition and inhibition by lysine. J. Biol. Chem. **281:** 31544–31552.

Kreft, O., Hoefgen, R., and Hesse, H. (2003). Functional analysis of cystathionine gamma-synthase in genetically engineered potato plants. Plant Physiol. **131:** 1843–1854.

Kwon, C., et al. (2008). Co-option of a default secretory pathway for plant immune responses. Nature **451:** 835–840.

Lee, M., Martin, M.N., Hudson, A.O., Lee, J., Muhitch, M.J., and Leustek, T. (2005). Methionine and threonine synthesis are limited by homoserine availability and not the activity of homoserine kinase in *Arabidopsis thaliana*. Plant J. **41:** 685–696.

Logemann, E., Birkenbihl, R.P., Ulker, B., and Somssich, I.E. (2006). An improved method for preparing Agrobacterium cells that simplifies the Arabidopsis transformation protocol. Plant Methods **2:** 16.

Lu, H., Rate, D.N., Song, J.T., and Greenberg, J.T. (2003). ACD6, a novel ankyrin protein, is a regulator and an effector of salicylic acid signaling in the *Arabidopsis* defense response. Plant Cell **15:** 2408–2420.

Mas-Droux, C., Curien, G., Robert-Genthon, M., Laurencin, M., Ferrer, J.L., and Dumas, R. (2006). A novel organization of ACT domains in allosteric enzymes revealed by the crystal structure of *Arabidopsis* aspartate kinase. Plant Cell **18:** 1681–1692.

Mikkelsen, M.D., Petersen, B.L., Glawischnig, E., Jensen, A.B., Andreasson, E., and Halkier, B.A. (2003). Modulation of CYP79 genes and glucosinolate profiles in *Arabidopsis* by defense signaling pathways. Plant Physiol. **131:** 298–308.

Muskett, P.R., Kahn, K., Austin, M.J., Moisan, L.J., Sadanandom, A., Shirasu, K., Jones, J.D.G., and Parker, J.E. (2002). Arabidopsis *RAR1* exerts rate-limiting control of *R* gene-mediated defenses against multiple pathogens. Plant Cell **14:** 979–992.

O'Connell, R.J., and Panstruga, R. (2006). Tête à tête inside a plant cell: Establishing compatibility between plants and biotrophic fungi and oomycetes. New Phytol. **171:** 699–718.

Parker, J.E., Coleman, M.J., Szabò, V., Frost, L.N., Schmidt, R., van der Biezen, E.A., Moores, T., Dean, C., Daniels, M.J., and Jones, J.D. (1997). The *Arabidopsis* downy mildew resistance gene *RPP5* shares similarity to the toll and interleukin-1 receptors with N and L6. Plant Cell **9:** 879–894.

Parker, J.E., Szabo, V., Staskawicz, B.J., Lister, C., Dean, C., Daniels, M., and Jones, J.D.G. (1993). Phenotypic characterization and molecular mapping of the *Arabidopsis thaliana* locus *RPP5*,

determining resistance to *Peronospora parasitica*. Plant J. **4:** 821–831.

Randall, T.A., et al. (2005). Large-scale gene discovery in the oomycete *Phytophthora infestans* reveals likely components of phytopathogenicity shared with true fungi. Mol. Plant Microbe Interact. **18:** 229–243.

Ravanel, S., Block, M.A., Rippert, P., Jabrin, S., Curien, G., Rébeillé, F., and Douce, R. (2004). Methionine metabolism in plants: Chloroplasts are autonomous for de novo methionine synthesis and can import S-adenosylmethionine from the cytosol. J. Biol. Chem. **279:** 22548–22557.

Rosso, M.G., Li, Y., Strizhov, N., Reiss, B., Dekker, K., and Weisshaar, B. (2003). An *Arabidopsis thaliana* T-DNA mutagenized population (GABI-Kat) for flanking sequence tag-based reverse genetics. Plant Mol. Biol. **53:** 247–259.

Sali, A., and Blundell, T.L. (1993). Comparative protein modelling by satisfaction of spatial restraints. J. Mol. Biol. **234:** 779–815.

Sanchez-Vallet, A., Ramos, B., Bednarek, P., López, G., Piślewska-Bednarek, M., Schulze-Lefert, P., and Molina, A. (2010). Tryptophan-derived secondary metabolites in *Arabidopsis thaliana* confer non-host resistance to necrotrophic *Plectosphaerella cucumerina* fungi. Plant J. **63:** 115–127.

Sarrobert, C., Thibaud, M.C., Contard-David, P., Gineste, S., Bechtold, N., Robaglia, C., and Nussaume, L. (2000). Identification of an *Arabidopsis thaliana* mutant accumulating threonine resulting from mutation in a new dihydrodipicolinate synthase gene. Plant J. **24:** 357–367.

Scheible, W.R., González-Fontes, A., Morcuende, R., Lauerer, M., Geiger, M., Glaab, J., Gojon, A., Schulze, E.D., and Stitt, M. (1997). Tobacco mutants with a decreased number of functional *nia* genes compensate by modifying the diurnal regulation of transcription, post-translational modification and turnover of nitrate reductase. Planta **203:** 304–319.

Schlaeppi, K., Abou-Mansour, E., Buchala, A., and Mauch, F. (2010). Disease resistance of *Arabidopsis* to *Phytophthora brassicae* is established by the sequential action of indole glucosinolates and camalexin. Plant J. **62:** 840–851.

Shirasu, K. (2009). The HSP90-SGT1 chaperone complex for NLR immune sensors. Annu. Rev. Plant Biol. **60:** 139–164.

Sinapidou, E., Williams, K., Nott, L., Bahkt, S., Tör, M., Crute, I., Bittner-Eddy, P., and Beynon, J. (2004). Two TIR:NB:LRR genes are required to specify resistance to *Peronospora parasitica* isolate Cala2 in *Arabidopsis*. Plant J. **38:** 898–909.

Smith, C.A., and Kortemme, T. (2008). Backrub-like backbone simulation recapitulates natural protein conformational variability and improves mutant side-chain prediction. J. Mol. Biol. **380:** 742–756.

Song, J.T., Lu, H., and Greenberg, J.T. (2004). Divergent roles in *Arabidopsis thaliana* development and defense of two homologous genes, *aberrant growth and death2* and *AGD2-LIKE DEFENSE RESPONSE PROTEIN1*, encoding novel aminotransferases. Plant Cell **16:** 353–366.

Spanu, P.D., et al. (2010). Genome expansion and gene loss in powdery mildew fungi reveal tradeoffs in extreme parasitism. Science **330:** 1543–1546.

Straus, M.R., Rietz, S., Ver Loren van Themaat, E., Bartsch, M., and Parker, J.E. (2010). Salicylic acid antagonism of EDS1-driven cell death is important for immune and oxidative stress responses in *Arabidopsis*. Plant J. **62:** 628–640.

Tornero, P., and Dangl, J.L. (2001). A high-throughput method for quantifying growth of phytopathogenic bacteria in *Arabidopsis thaliana*. Plant J. **28:** 475–481.

Tyler, B.M., et al. (2006). *Phytophthora* genome sequences uncover evolutionary origins and mechanisms of pathogenesis. Science **313:** 1261–1266.

van Damme, M., Zeilmaker, T., Elberse, J., Andel, A., de Sain-van der Velden, M., and van den Ackerveken, G. (2009). Downy mildew resistance in Arabidopsis by mutation of *HOMOSERINE KINASE*. Plant Cell **21:** 2179–2189.

Vauterin, M., Frankard, V., and Jacobs, M. (2000). Functional rescue of a bacterial *dapA* auxotroph with a plant cDNA library selects for mutant clones encoding a feedback-insensitive dihydrodipicolinate synthase. Plant J. **21:** 239–248.

Vlot, A.C., Dempsey, D.A., and Klessig, D.F. (2009). Salicylic acid, a multifaceted hormone to combat disease. Annu. Rev. Phytopathol. **47:** 177–206.

Wang, W., Wen, Y., Berkey, R., and Xiao, S. (2009). Specific targeting of the *Arabidopsis* resistance protein RPW8.2 to the interfacial membrane encasing the fungal Haustorium renders broad-spectrum resistance to powdery mildew. Plant Cell **21:** 2898–2913.

Whisson, S.C., et al. (2007). A translocation signal for delivery of oomycete effector proteins into host plant cells. Nature **450:** 115–118.

Wirthmueller, L., Zhang, Y., Jones, J.D., and Parker, J.E. (2007). Nuclear accumulation of the *Arabidopsis* immune receptor RPS4 is necessary for triggering EDS1-dependent defense. Curr. Biol. **17:** 2023–2029.

Xu, H., Andi, B., Qian, J., West, A.H., and Cook, P.F. (2006). The alpha-aminoadipate pathway for lysine biosynthesis in fungi. Cell Biochem. Biophys. **46:** 43–64.

Zhang, M., Kadota, Y., Prodromou, C., Shirasu, K., and Pearl, L.H. (2010). Structural basis for assembly of Hsp90-Sgt1-CHORD protein complexes: Implications for chaperoning of NLR innate immunity receptors. Mol. Cell **39:** 269–281.

Zhang, Y.L., Goritschnig, S., Dong, X.N., and Li, X. (2003). A gain-of-function mutation in a plant disease resistance gene leads to constitutive activation of downstream signal transduction pathways in *suppressor of npr1-1, constitutive 1*. Plant Cell **15:** 2636–2646.

Zhao, Y., Hull, A.K., Gupta, N.R., Goss, K.A., Alonso, J., Ecker, J.R., Normanly, J., Chory, J., and Celenza, J.L. (2002). Trp-dependent auxin biosynthesis in Arabidopsis: involvement of cytochrome P450s CYP79B2 and CYP79B3. Genes Dev. **16:** 3100–3112.